Electronic Supplementary Information

For

Synthesis, Characterization, and Alkoxide Transfer Reactivity of Dimeric $Tl_2(OR)_2$ Complexes

Amanda Grass,[a†] Lakshani Wathsala Kulathungage,[a†] Duleeka Wannipurage,[a†] Maryam Yousif,[a,c] Cassandra L. Ward,[b] Stanislav Groysman[*a]

[a]Department of Chemistry, Wayne State University, 5101 Cass Ave. Detroit MI 48202.

[b]Lumigen Instrument Center, Wayne State University, 5101 Cass Avenue, Detroit, Michigan 48202, United States.

[c]Current affiliation: Department of Chemistry, Grand Valley State University. 1 Campus Drive, 312 Padnos Hall, Allendale, Michigan 49401

E-mail: groysman@wayne.edu

[†]These authors contributed equally to this work.

Table of Contents

1. NMR Spectra

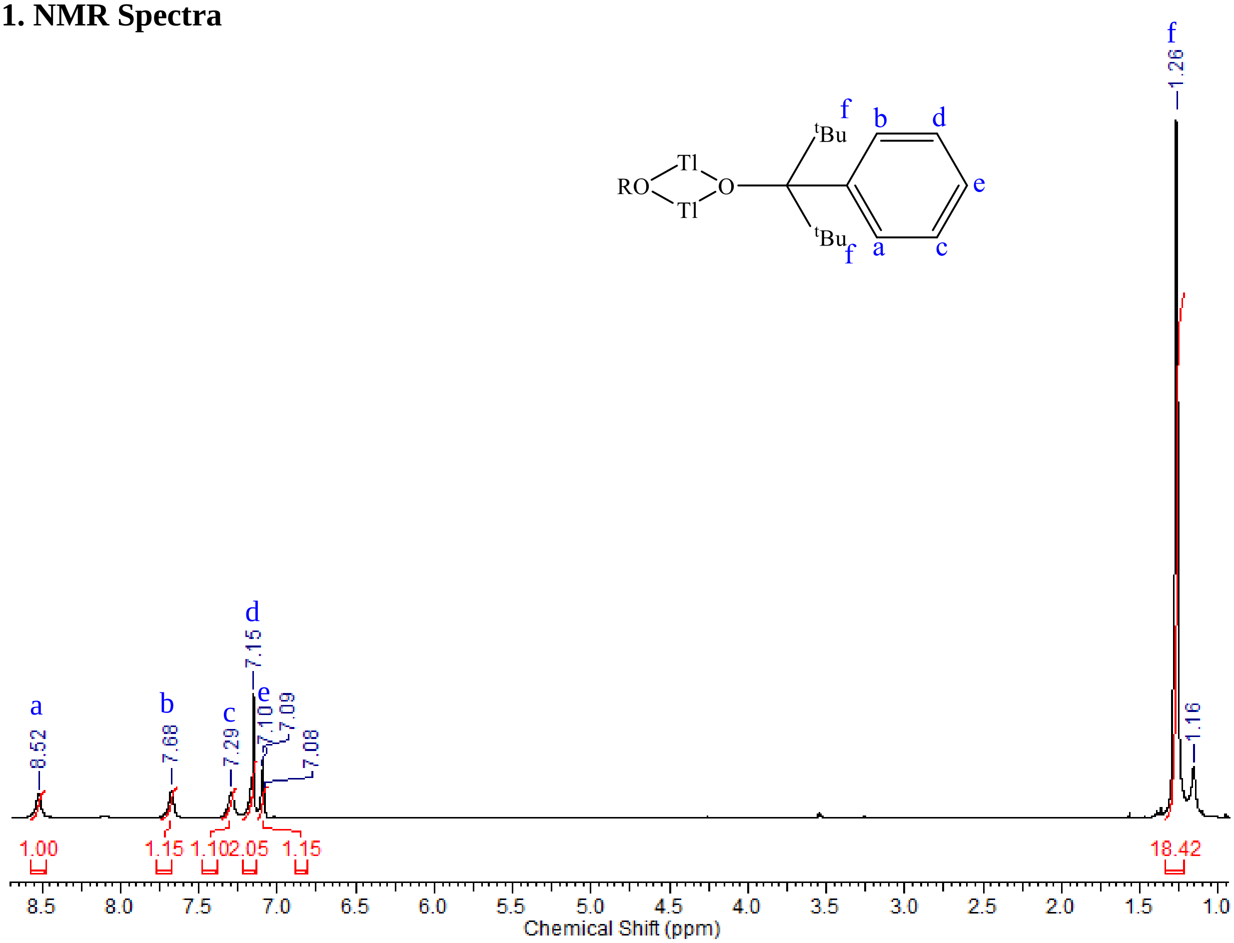

Figure S1. [1]H NMR of $Tl_2(OC^tBu_2Ph)_2$ (C_6D_6, 600 MHz, room temperature).

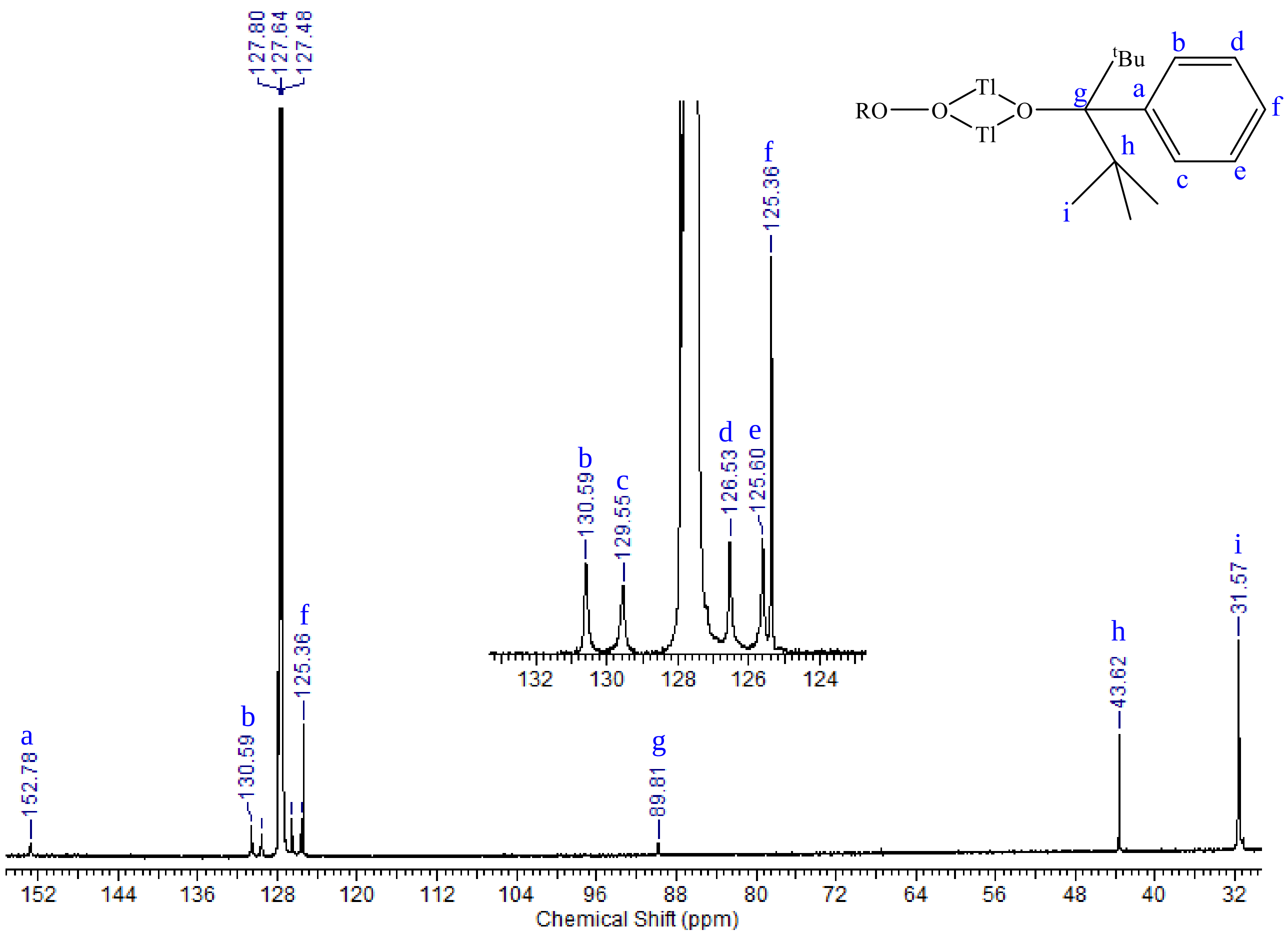

Figure S2. ^{13}C NMR of $Tl_2(OC^tBu_2Ph)_2$ (C_6D_6, 150 MHz).

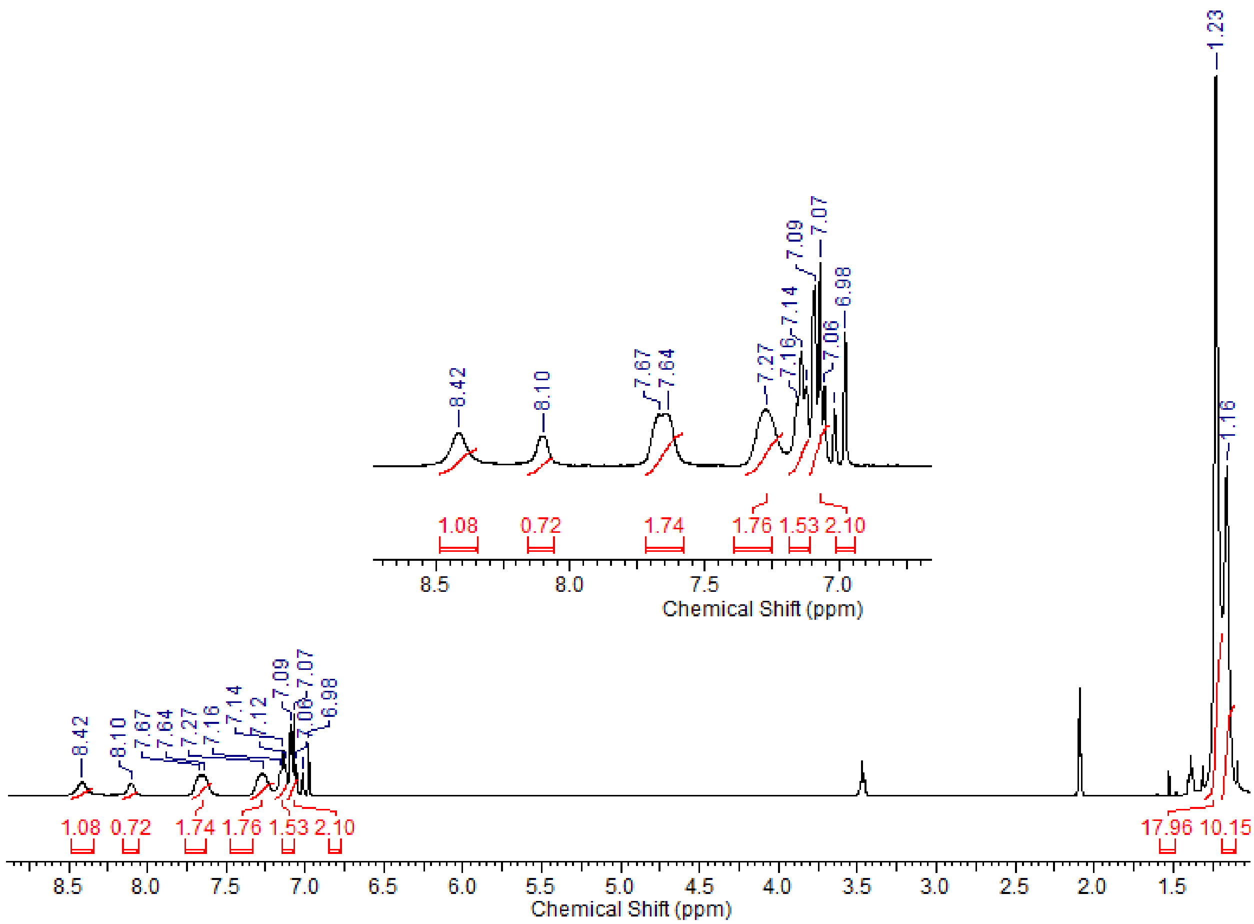

Figure S3. ^{1}H NMR of $Tl_2(OC^tBu_2Ph)_2$ (C_7D_8, 400 MHz, room temperature).

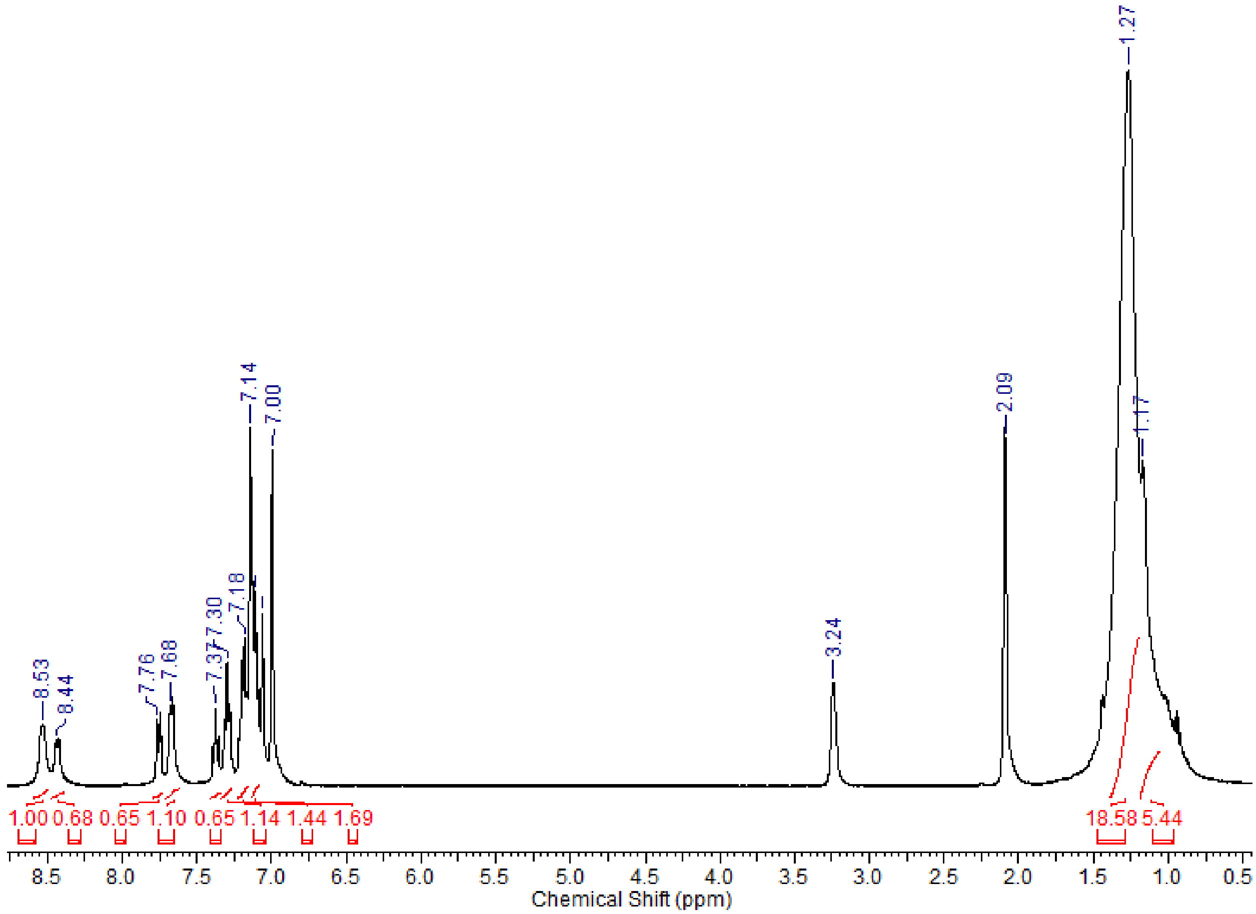

Figure S4. ^{1}H NMR of $Tl_2(OC^tBu_2Ph)_2$ (C_7D_8, 400 MHz, -40 ^{0}C).

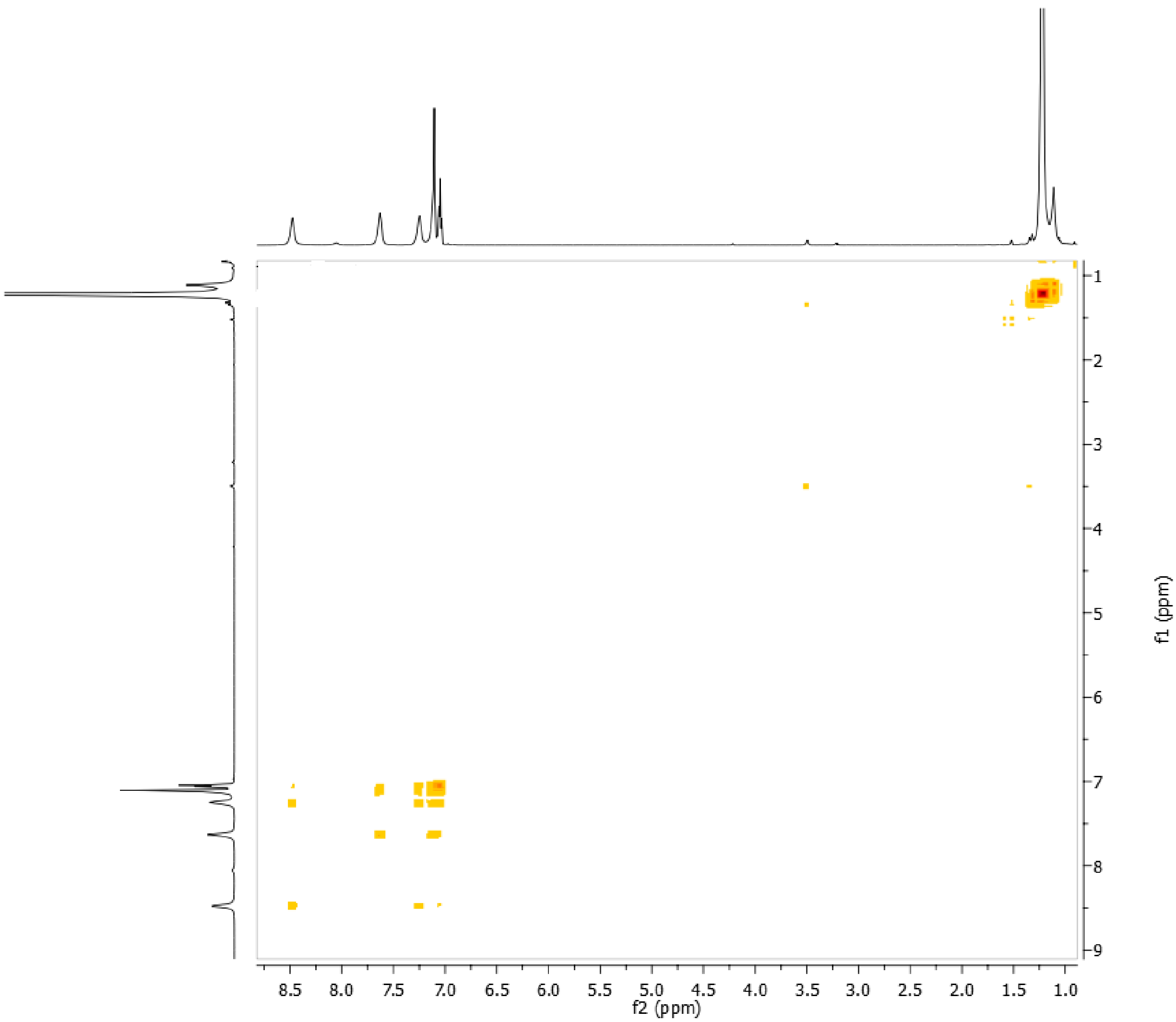

Figure S5. ^{1}H-^{1}H COSY NMR of $Tl_2(OC^tBu_2Ph)_2$ (C_6D_6, 600 MHz).

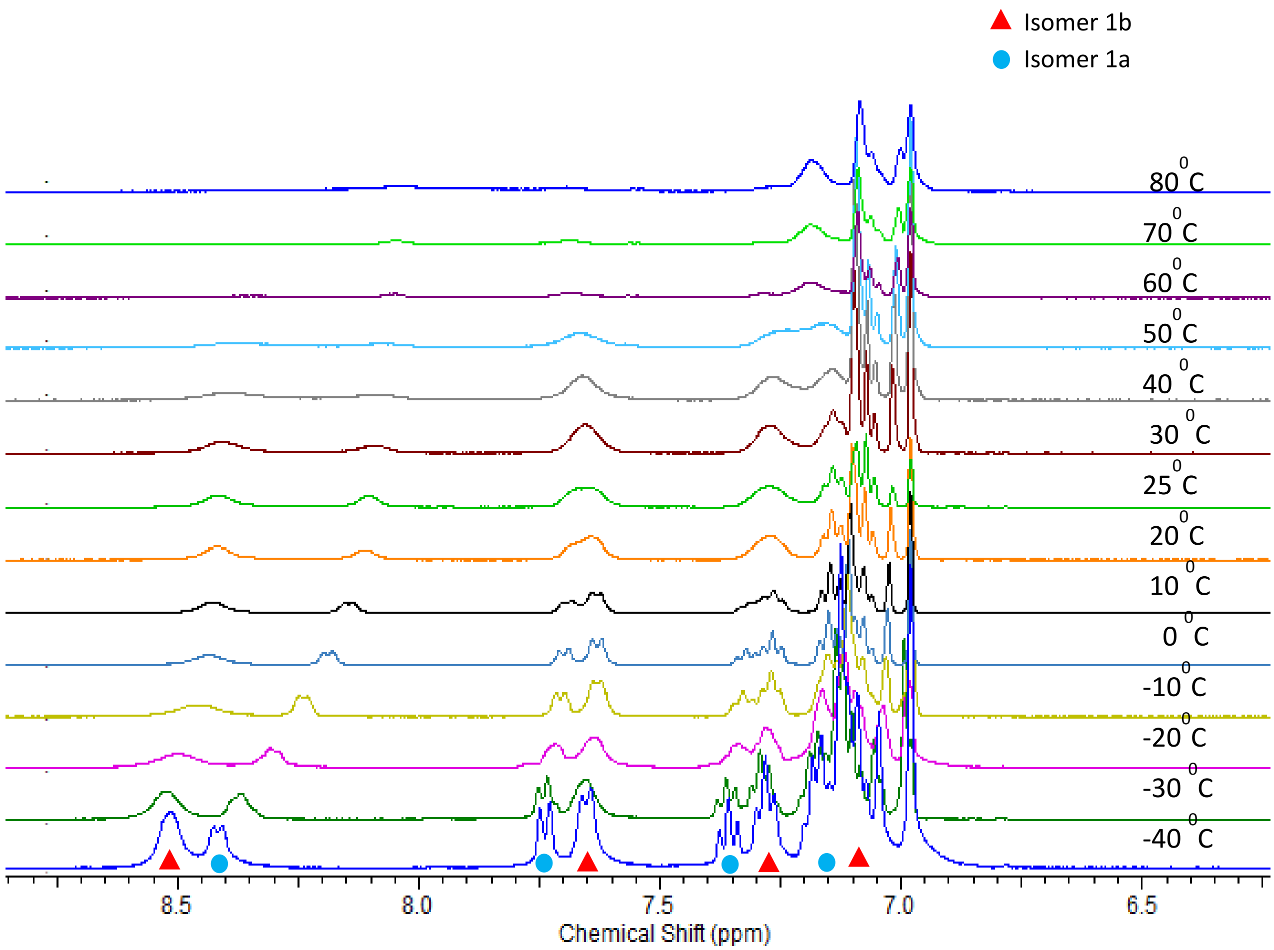

Figure S6. VT ^{1}H NMR of $Tl_2(OC^tBu_2Ph)_2$ (C_7D_8, 400 MHz).

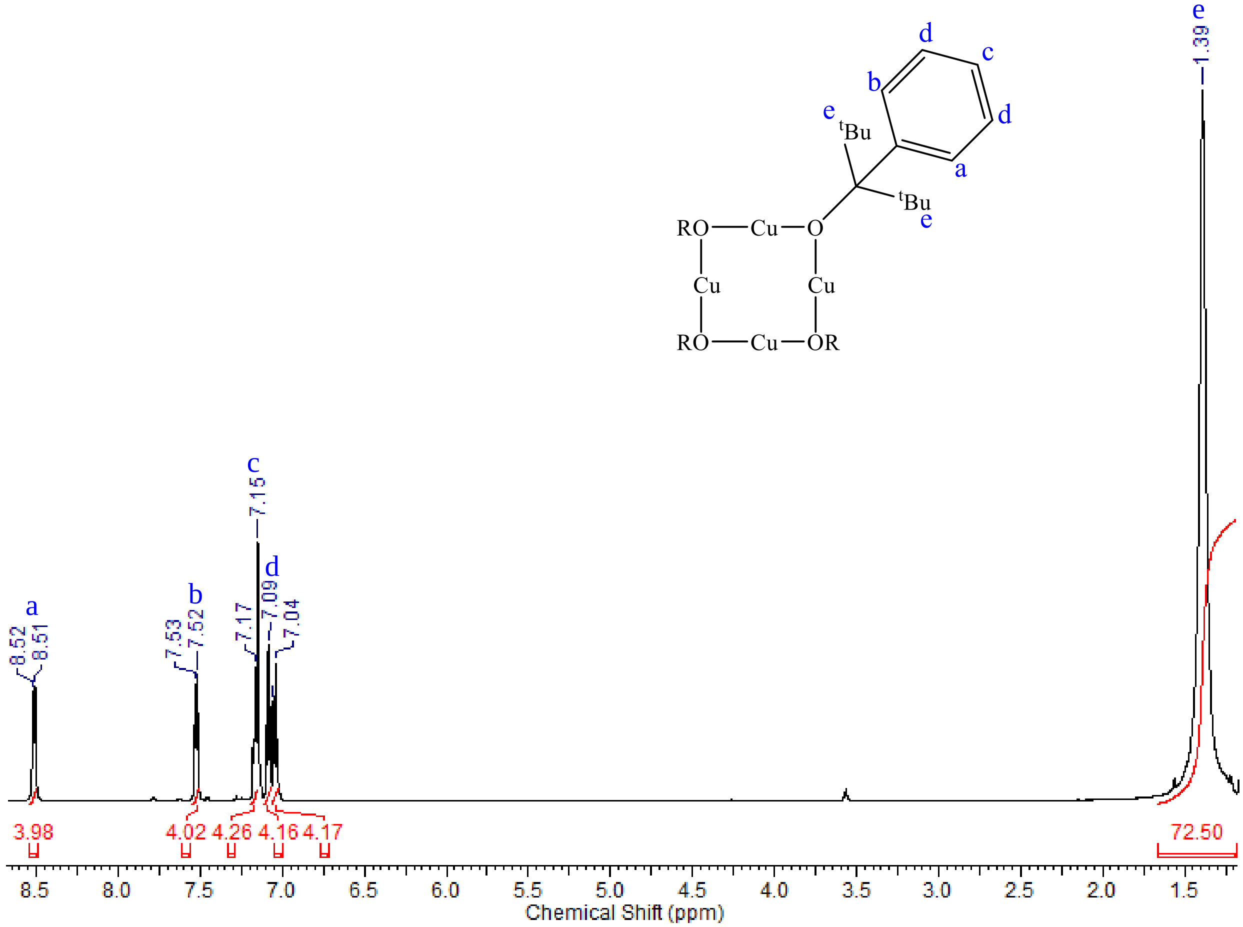

Figure S7. ^{1}H NMR of $Cu_4(OC^tBu_2Ph)_4$ (C_6D_6, 600 MHz).

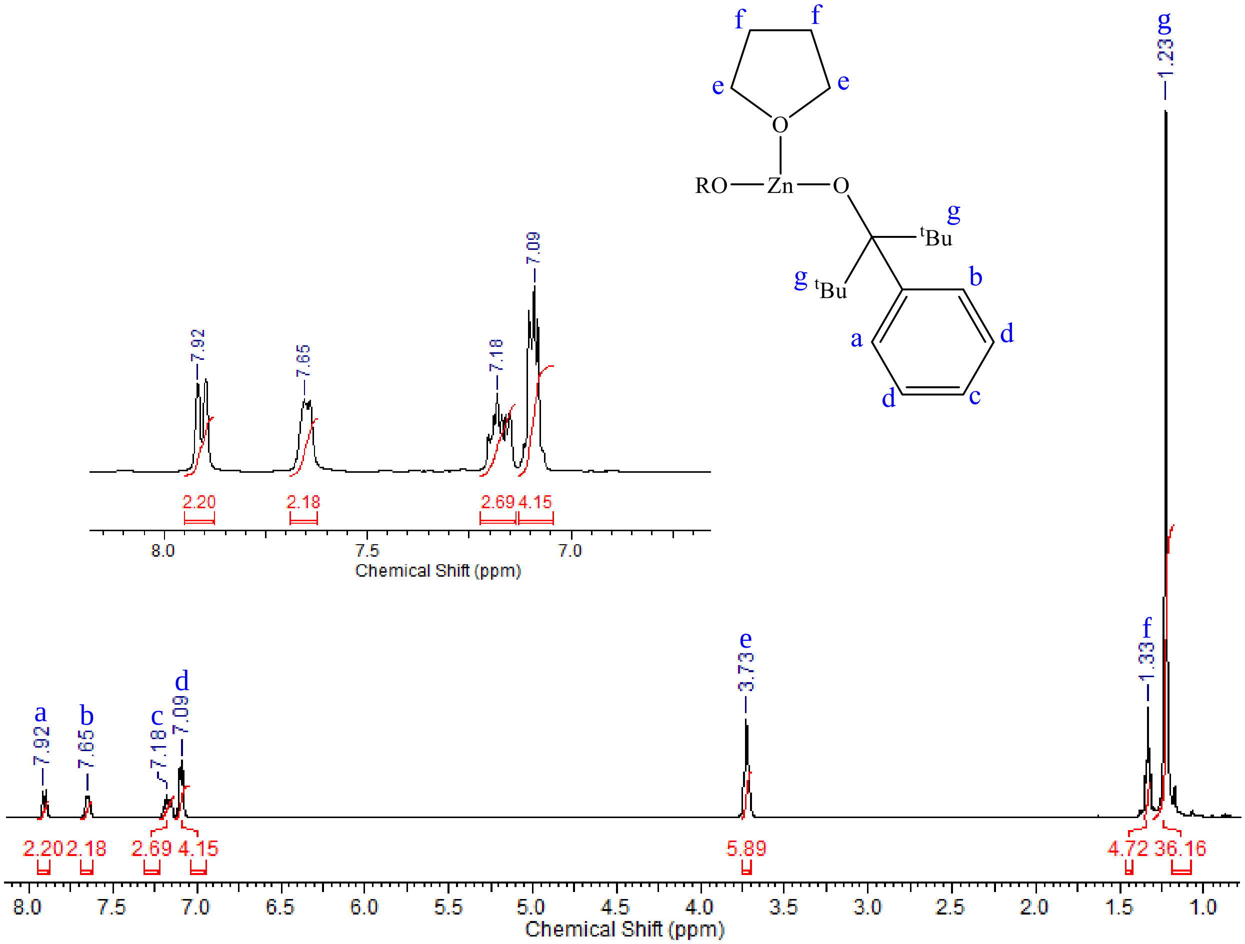

Figure S8. ^{1}H NMR of Zn(OC^{t}Bu$_2$Ph)$_2$(THF) (C_6D_6, 400 MHz).

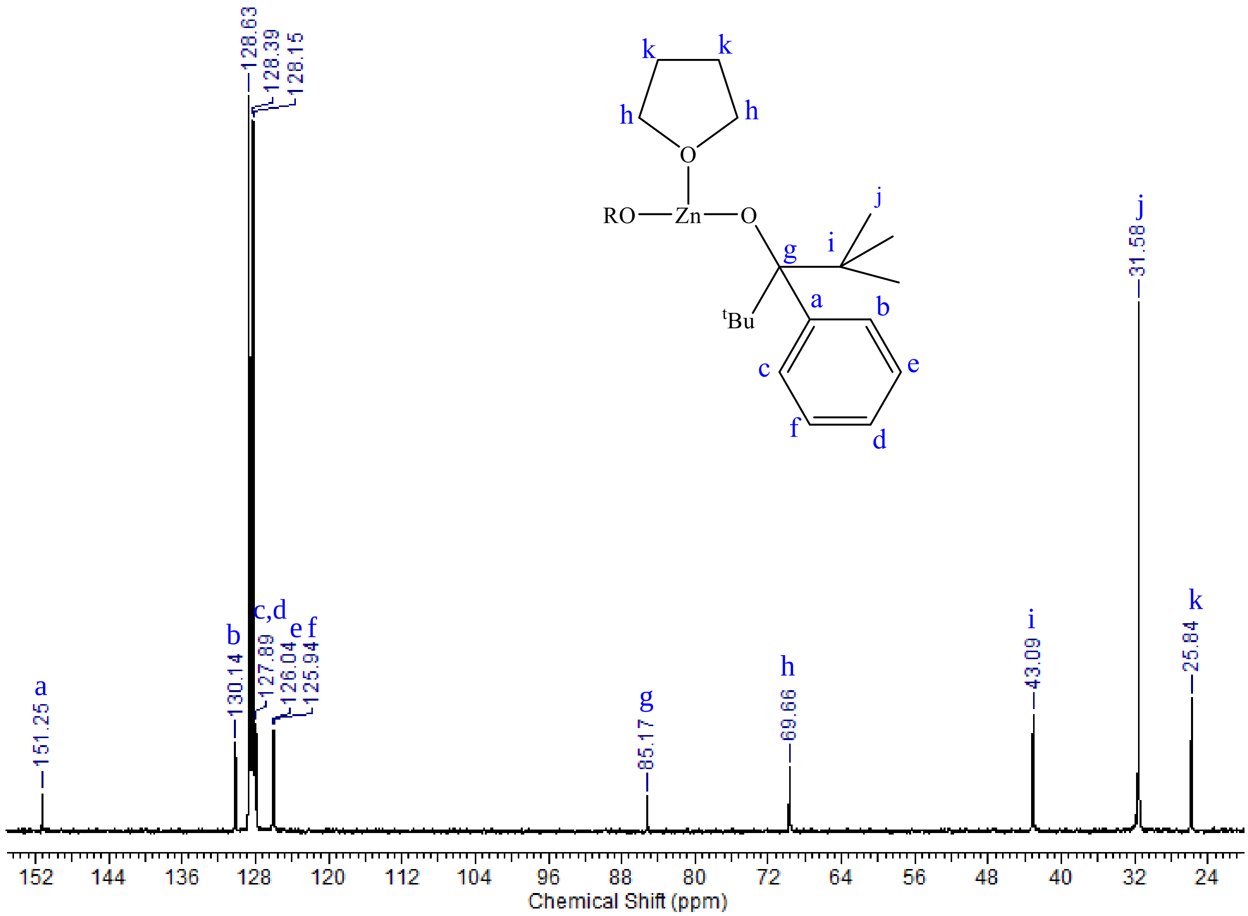

Figure S9. ^{13}C NMR of $Zn(OR)_2(THF)$ (C_6D_6, 100 MHz).

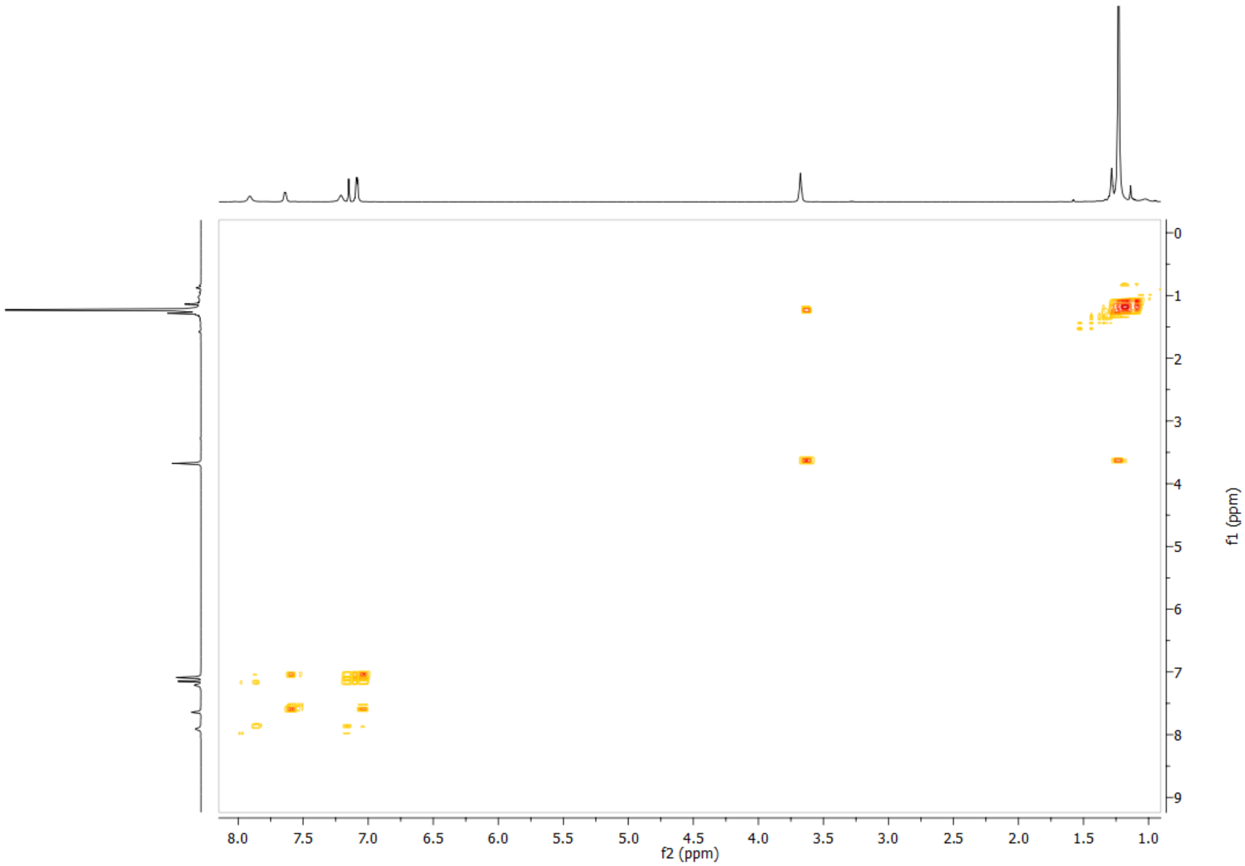

Figure S10. ^{1}H-^{1}H COSY NMR of $Zn(OR)_2(THF)$ (C_6D_6, 600 MHz).

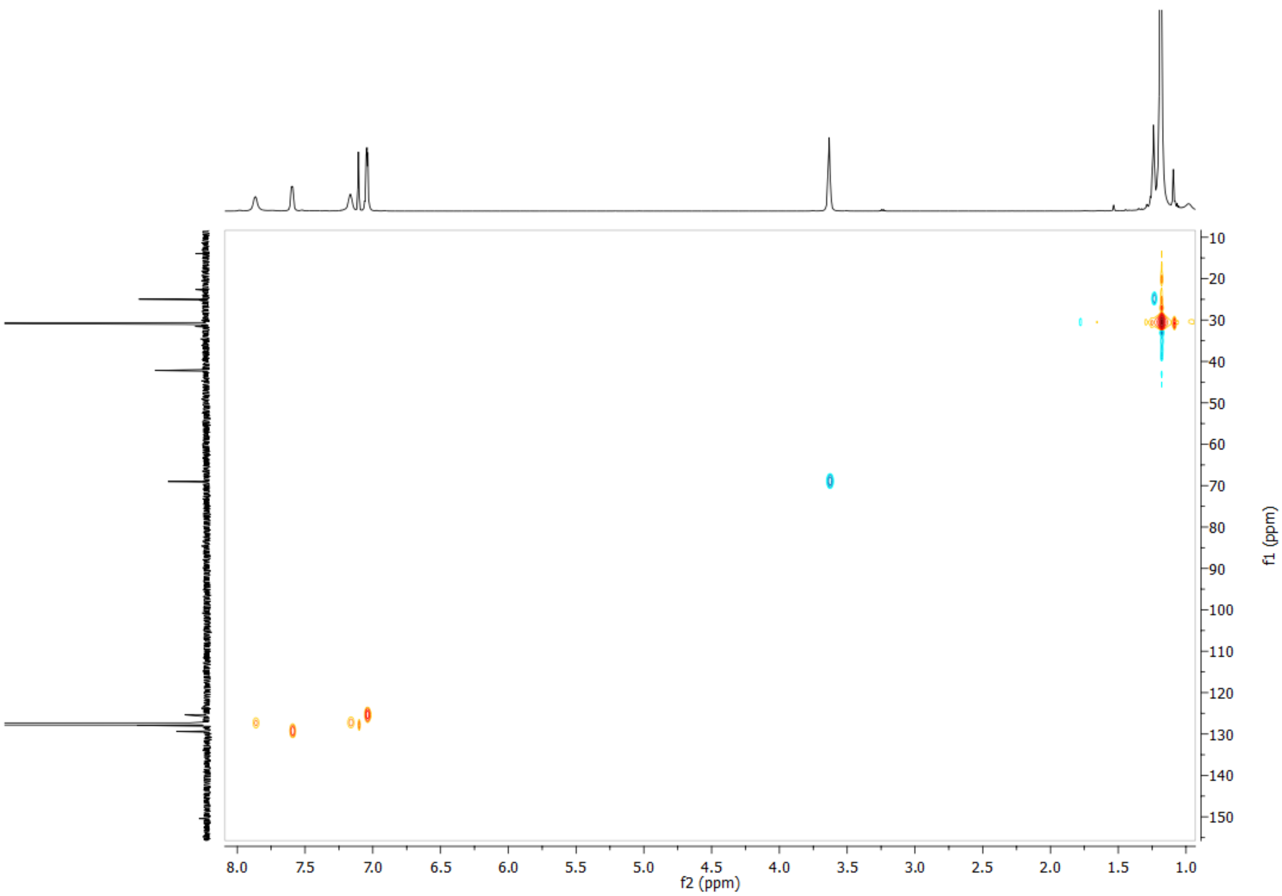

Figure S11. ^{1}H-^{13}C HSQCAD NMR of $Zn(OR)_2(THF)$ (C_6D_6, 600 MHz).

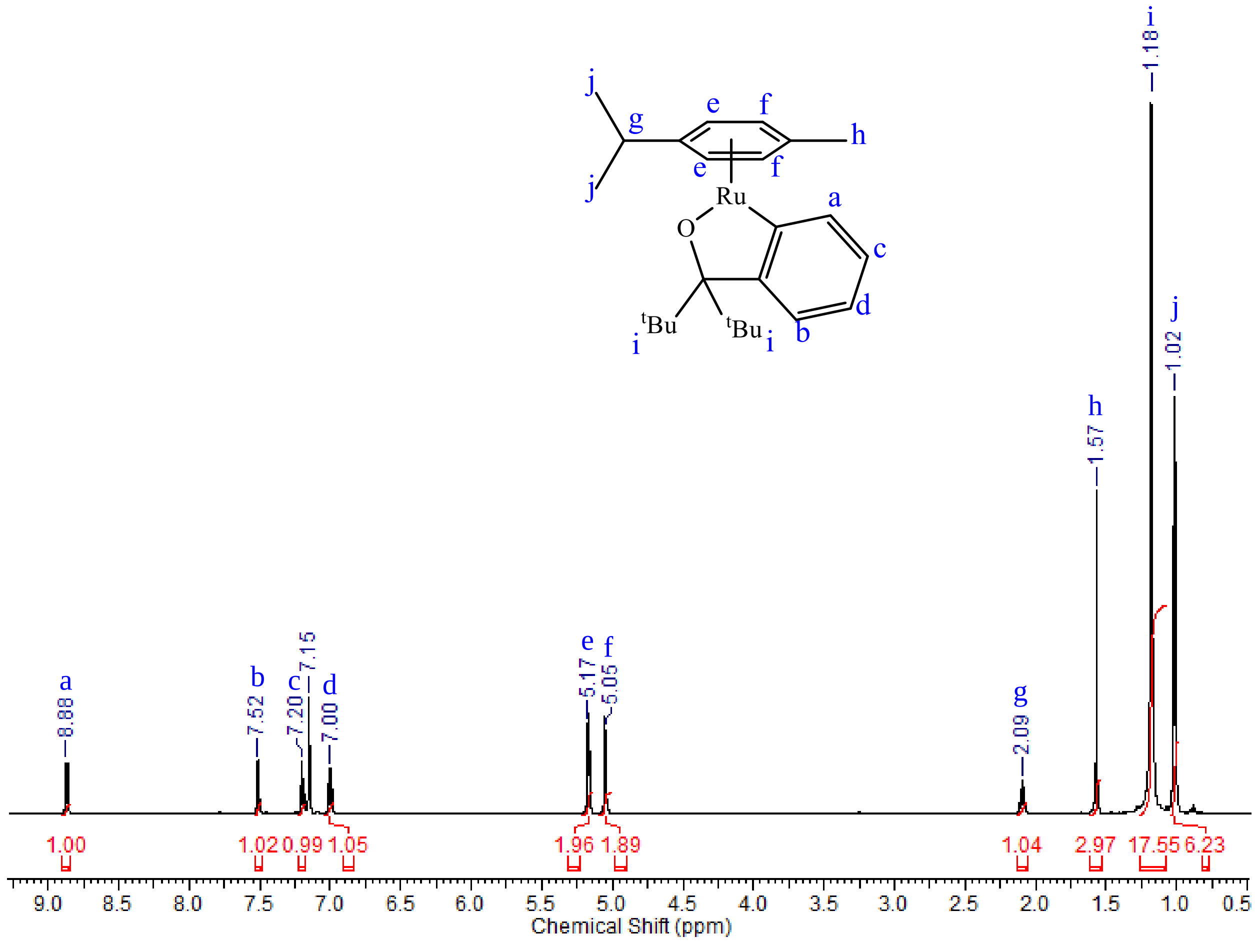

Figure S12. ^{1}H NMR of Ru(cymene)(κ^2-OC^{t}Bu$_2$C$_6$H$_2$) (C_6D_6, 600 MHz).

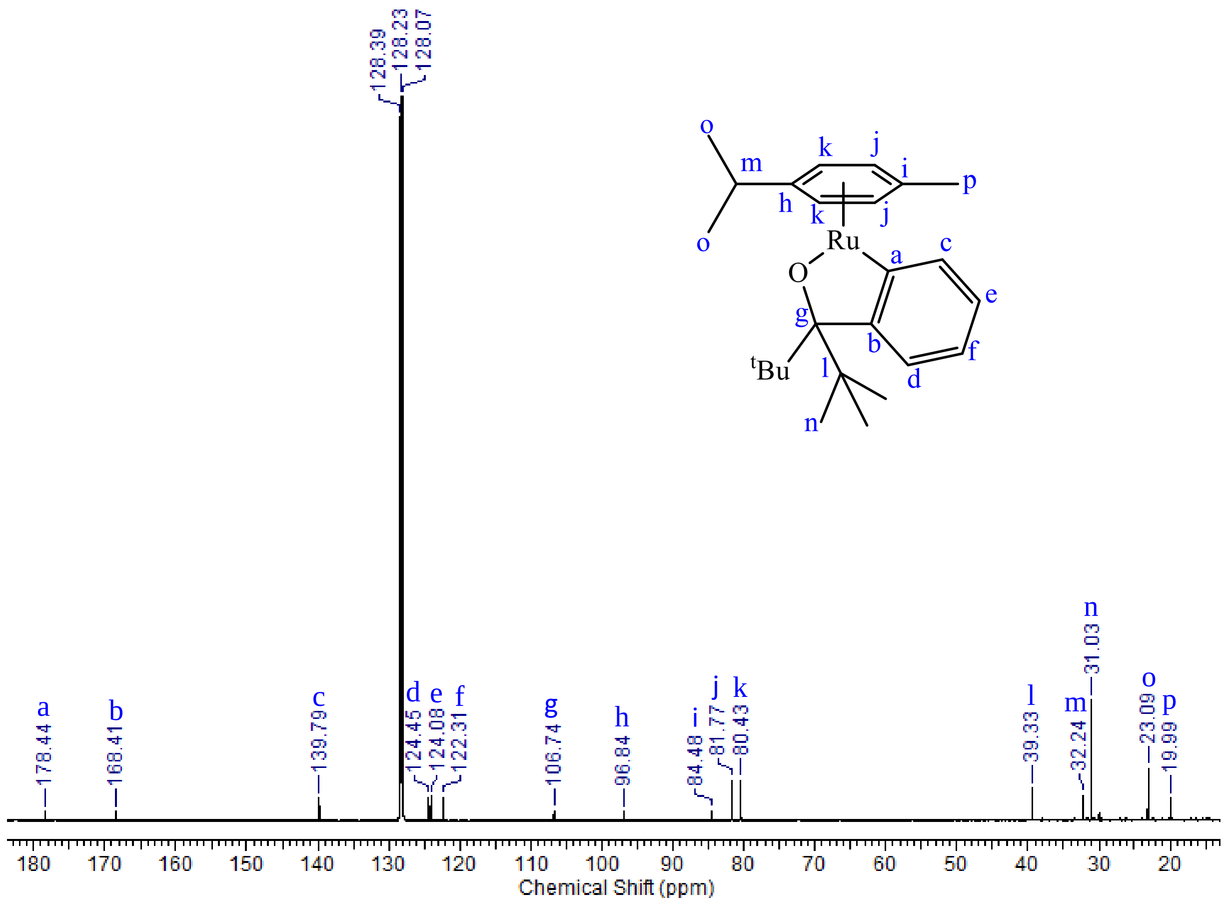

Figure S13. ^{13}C NMR of Ru(cymene)(κ^2-OC^{t}Bu$_2$C$_6$H$_2$) (C_6D_6, 150 MHz).

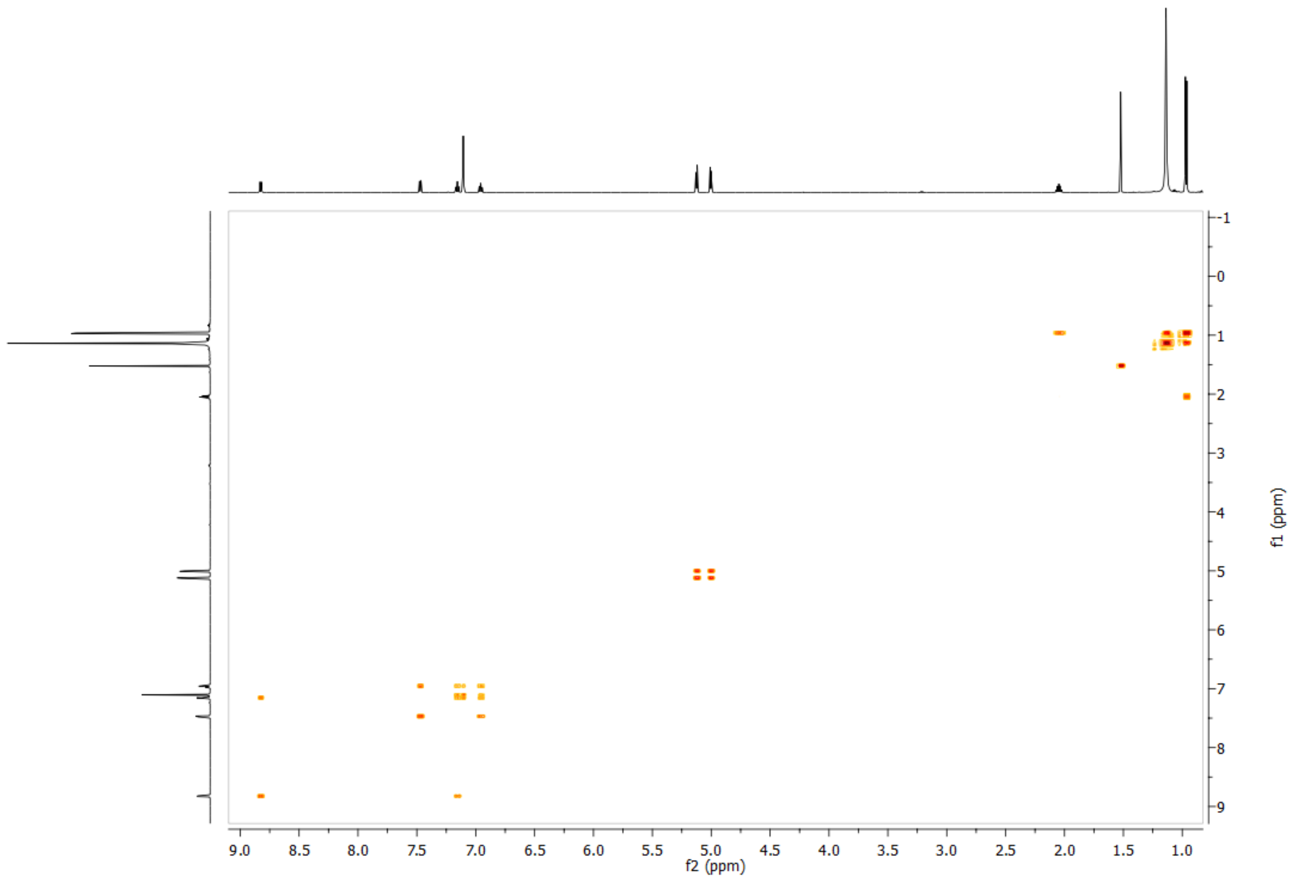

Figure S14. ^{1}H-^{1}H COSY NMR of Ru(cymene)(κ^2-OC^{t}Bu$_2$C$_6$H$_2$) (C_6D_6, 600 MHz).

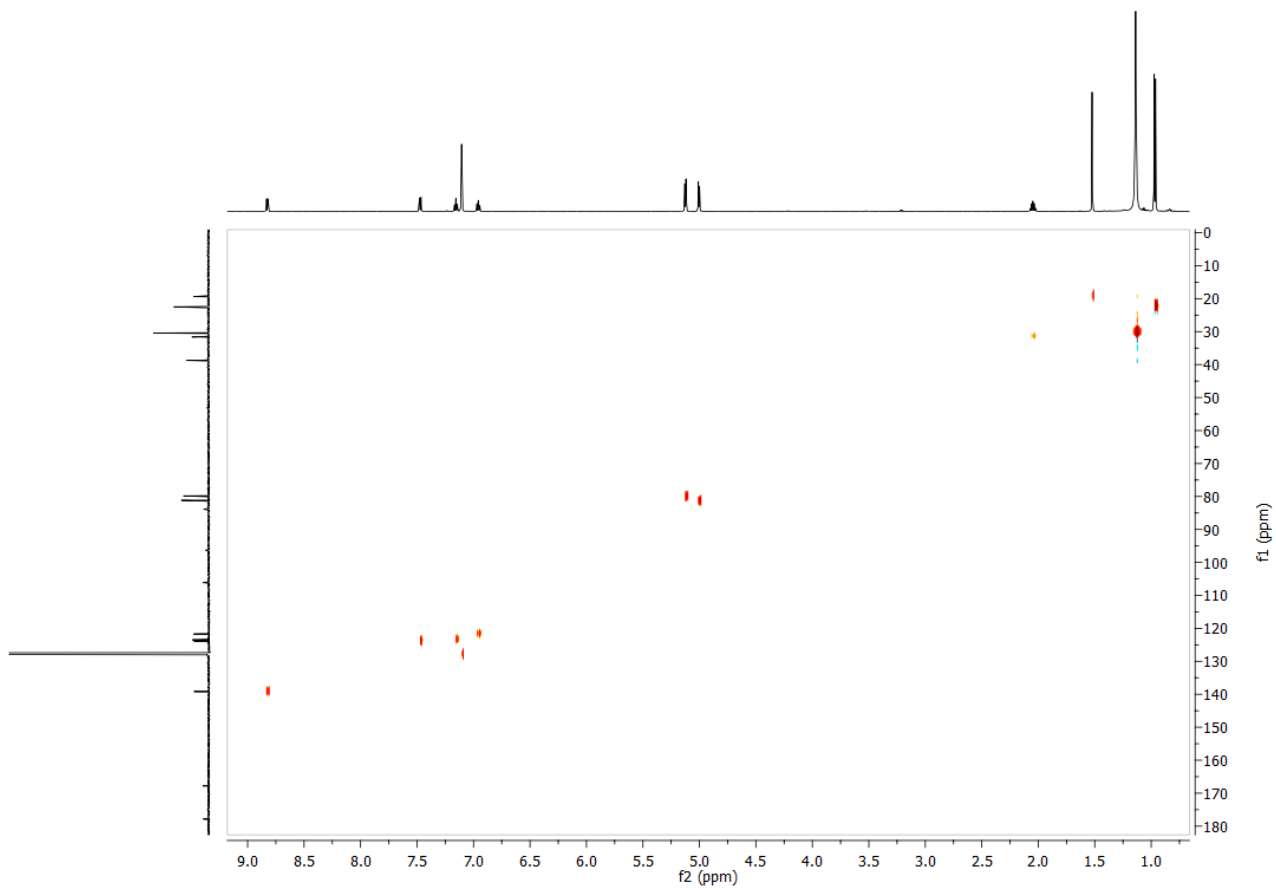

Figure S15. ^{1}H-^{13}C HSQCAD NMR of Ru(cymene)(κ^2-OC^{t}Bu$_2$C$_6$H$_2$) (C$_6$D$_6$, 600 MHz).

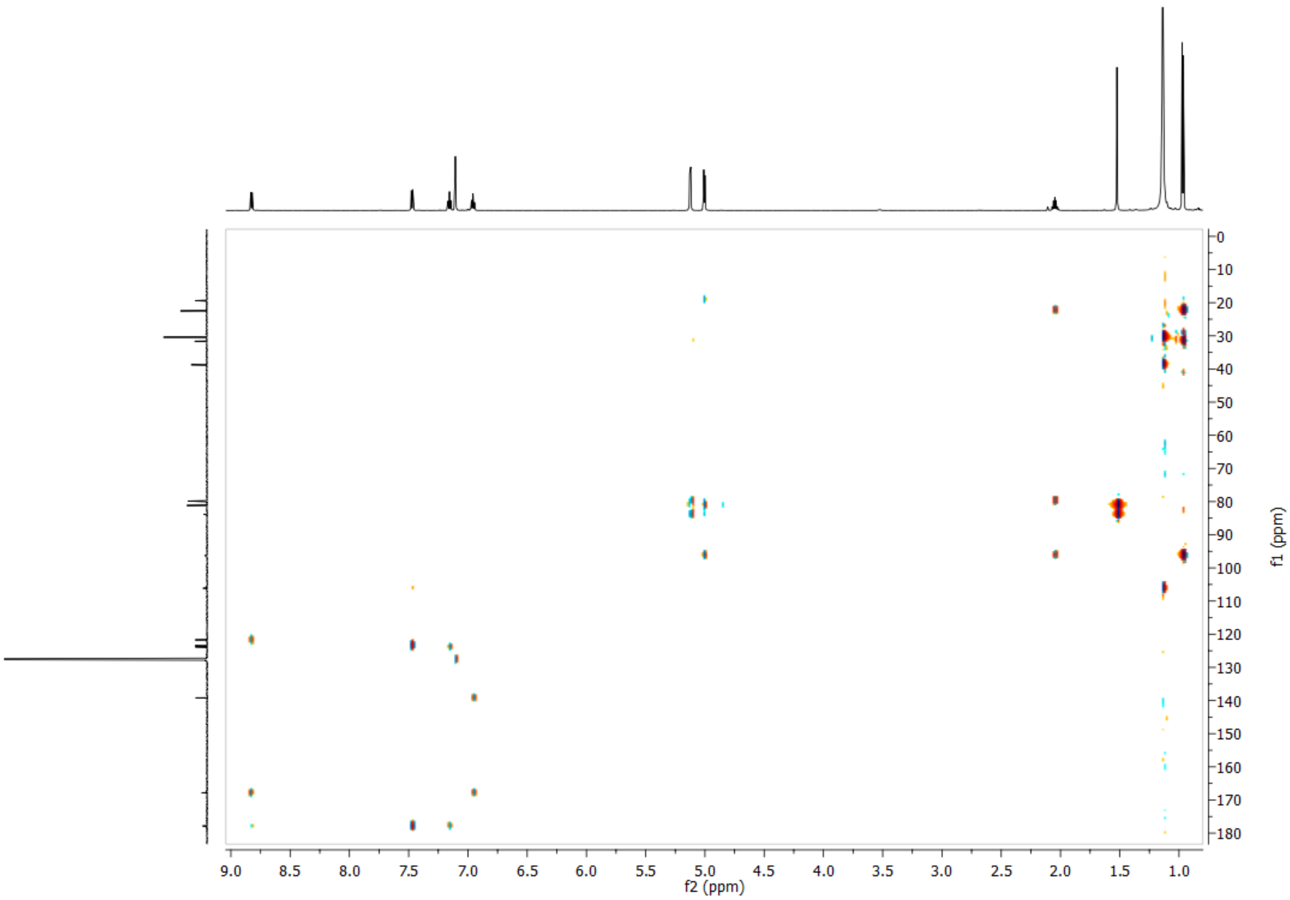

Figure S16. ^{1}H-^{13}C HMBC NMR of Ru(cymene)(κ^2-OC^{t}Bu$_2$C$_6$H$_2$) (C_6D_6, 600 MHz).

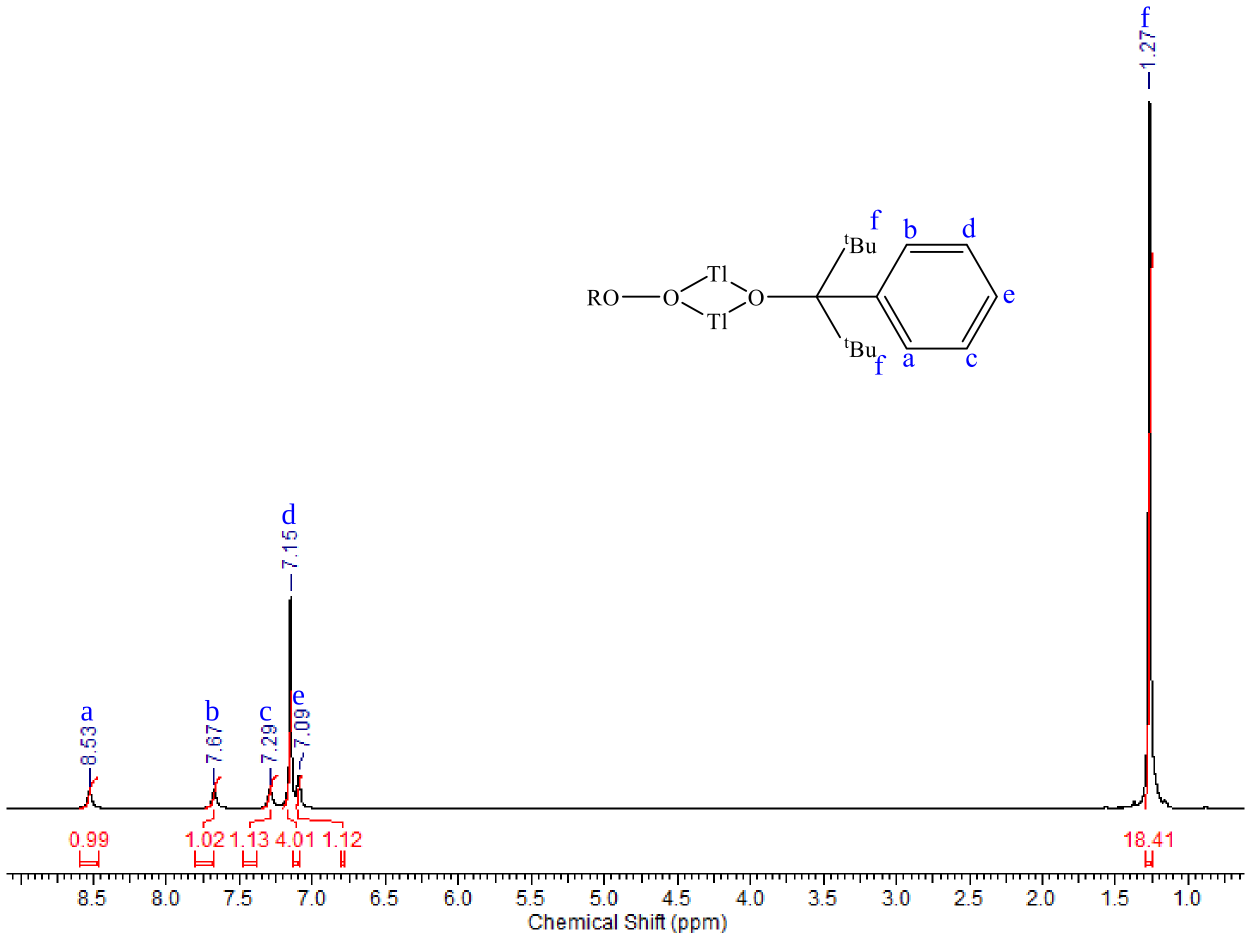

Figure S17. [1]H NMR of $Tl_2(OC^tBu_2Ph)_2$ as obtained from the attempted preparation of "$Ni(OR)_2$" (C_6D_6, 600 MHz).

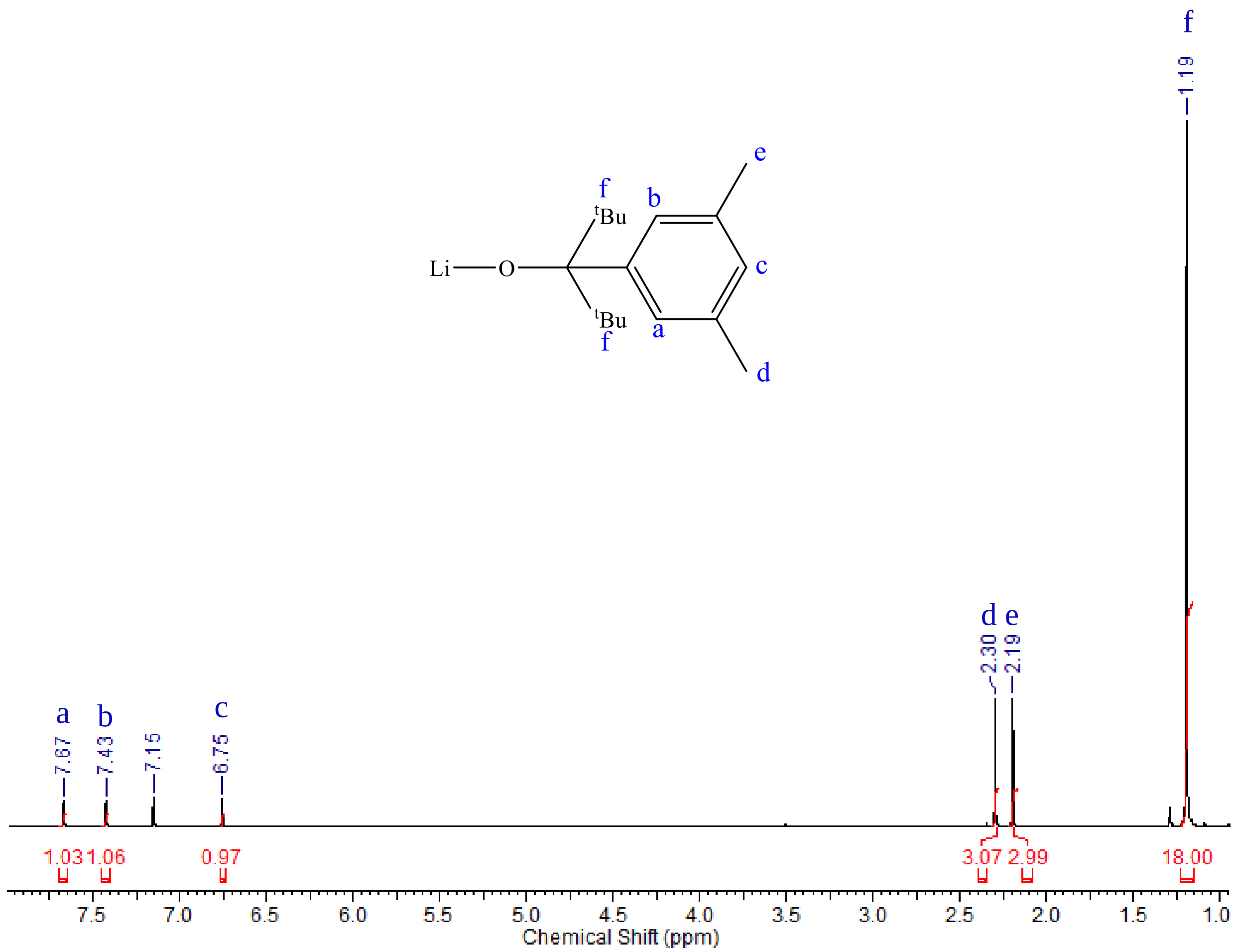

Figure S18. ^{1}H NMR of LiOC^{t}Bu$_2$(3,5-Me$_2$C$_6$H$_3$) (C_6D_6, 600 MHz).

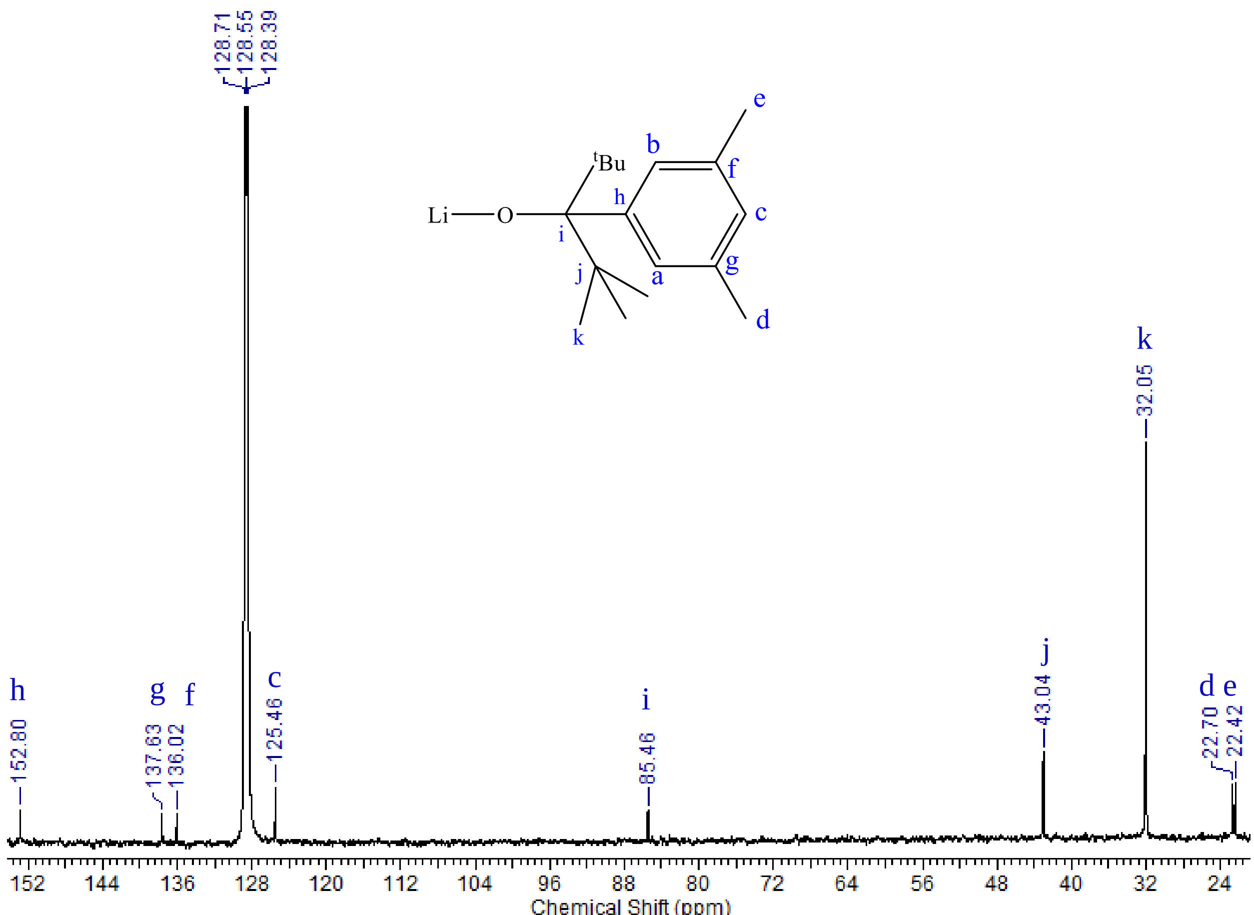

Figure S19. ^{13}C NMR of LiOC^{t}Bu$_2$(3,5-Me$_2$C$_6$H$_3$) (C_6D_6, 150 MHz). *Carbons **a** and **b** appear under C_6D_6 peaks, and were detected by HSQCAD, HMBC and HMQC.

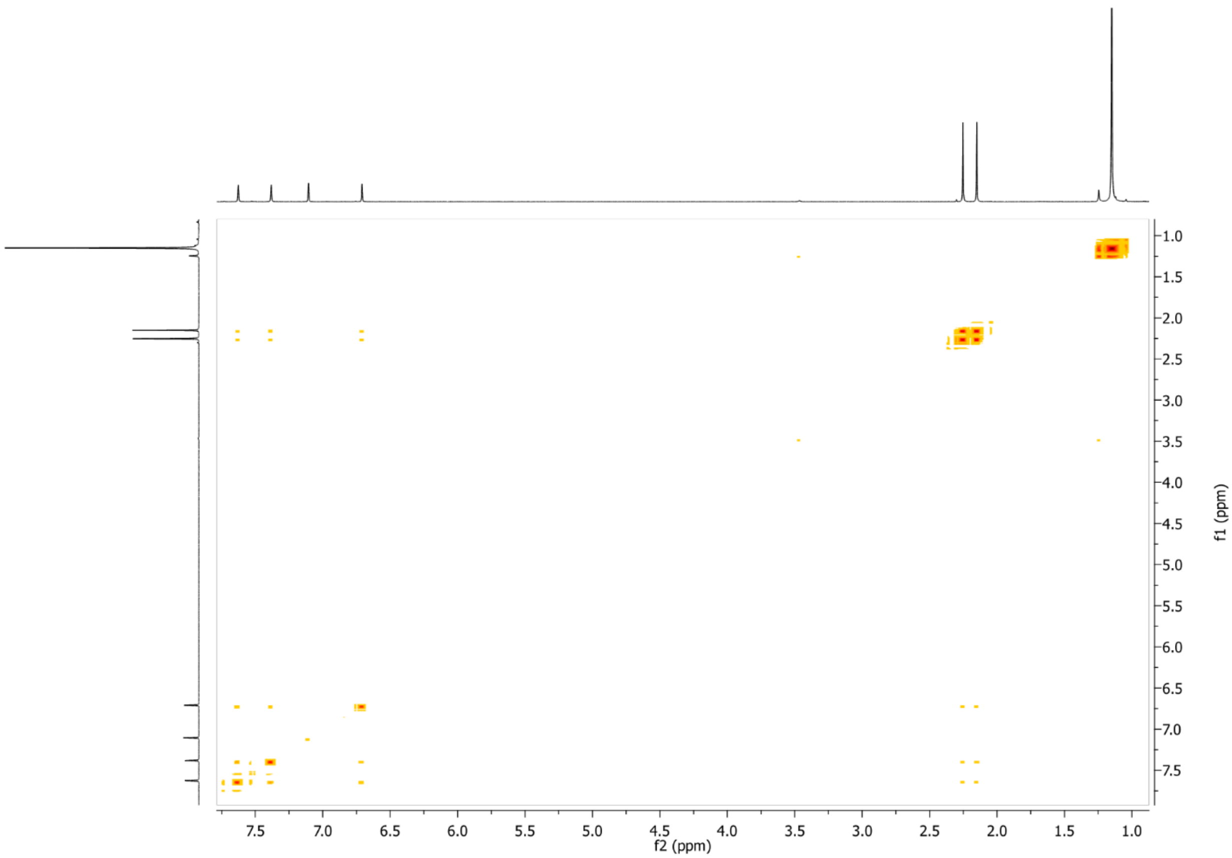

Figure S20. [1]H-[1]H COSY NMR of $LiOC^{t}Bu_2(3,5\text{-}Me_2C_6H_3)$ (C_6D_6, 600 MHz).

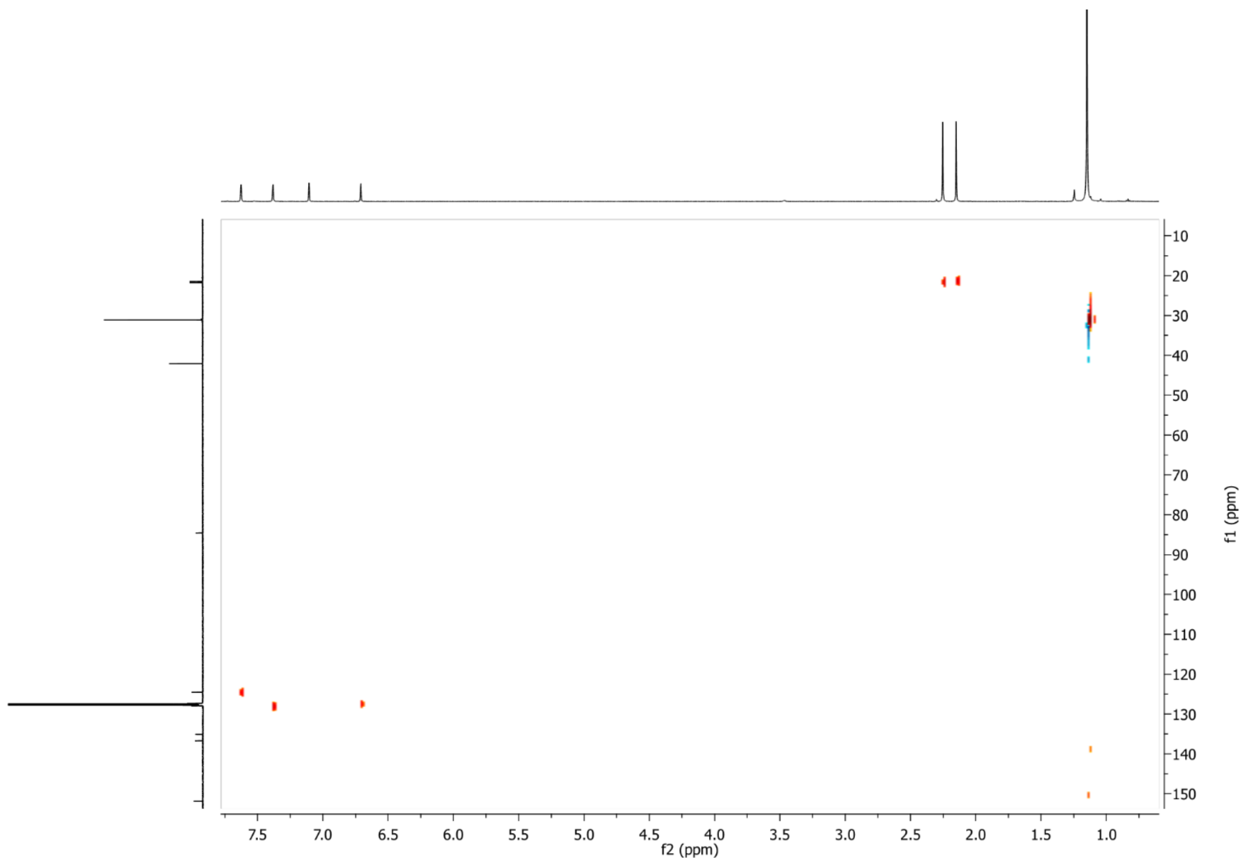

Figure S21. ^{1}H-^{13}C HSQCAD NMR of $LiOC^{t}Bu_2(3,5\text{-}Me_2C_6H_3)$ (C_6D_6, 600 MHz).

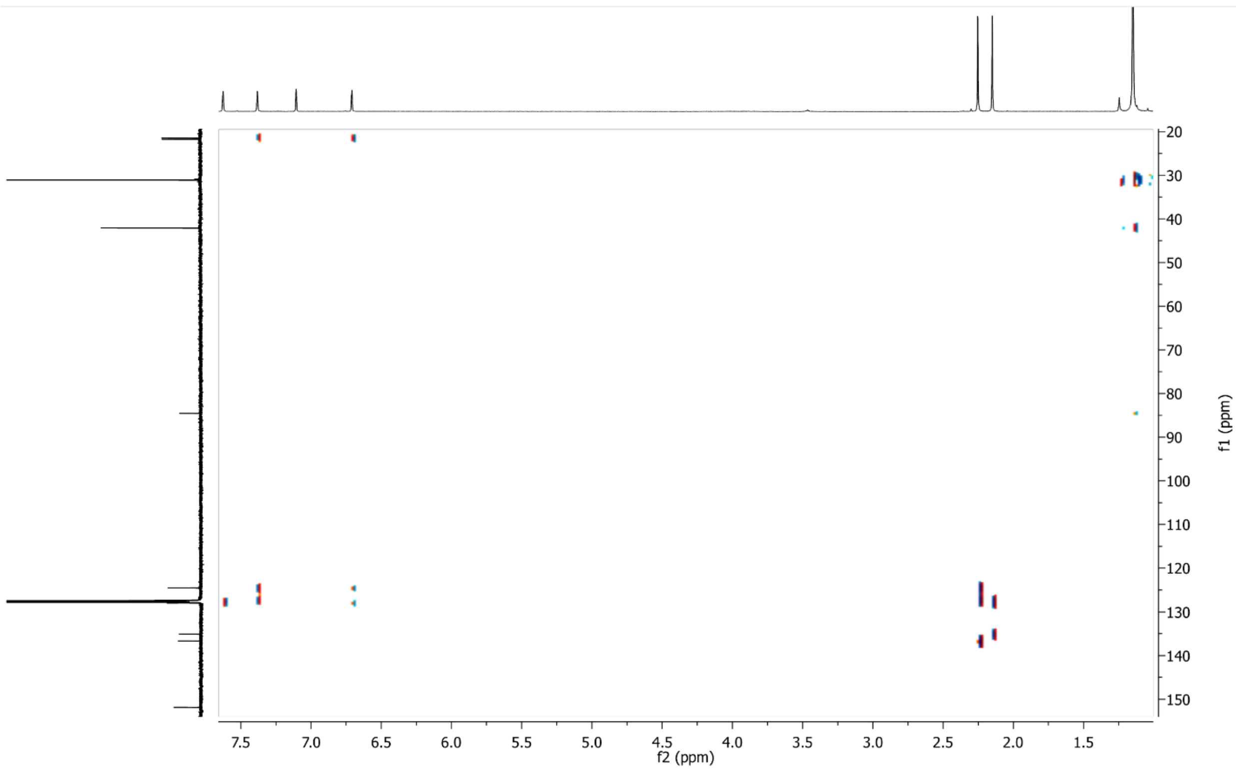

Figure S22. ^{1}H-^{13}C HMBCAD NMR of $LiOC^{t}Bu_2(3,5\text{-}Me_2C_6H_3)$ (C_6D_6, 600 MHz).

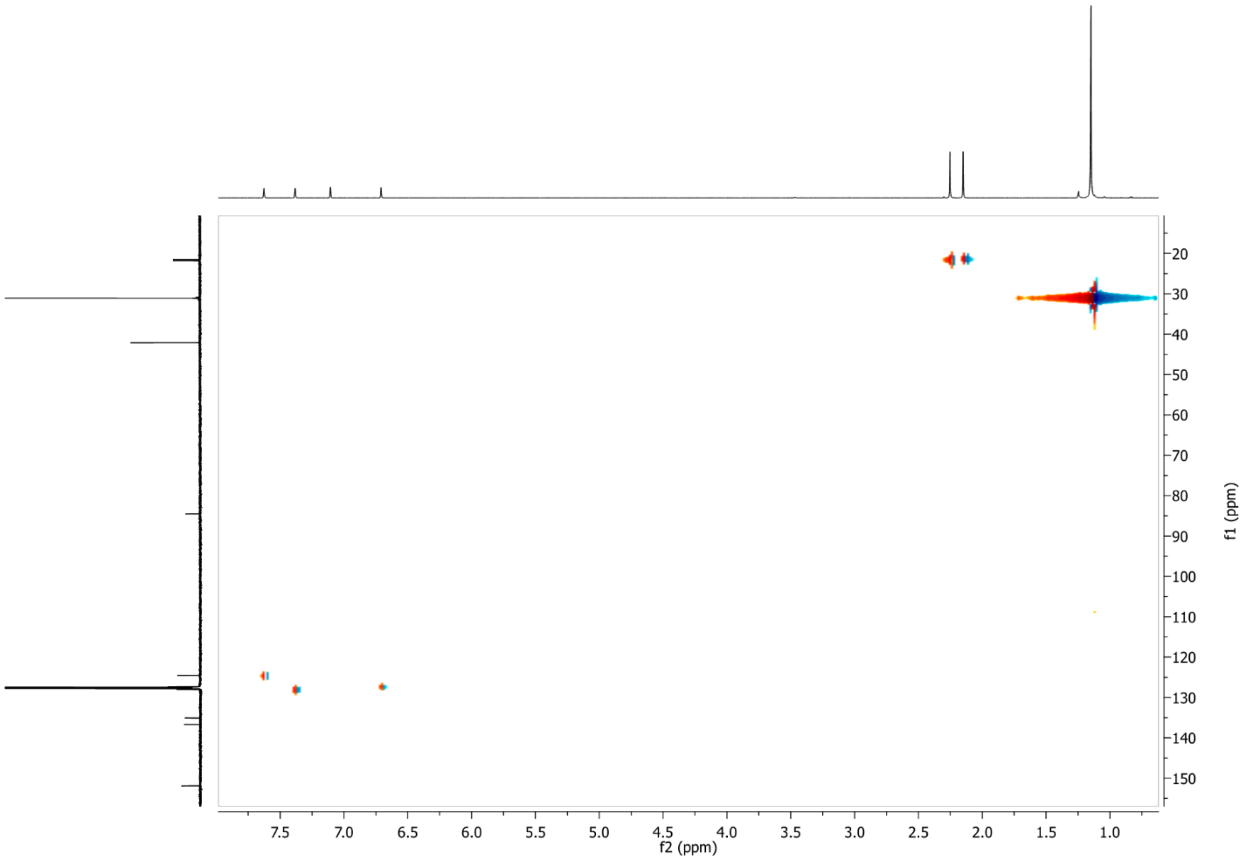

Figure S23. ^{1}H-^{13}C HMQC NMR of $LiOC^tBu_2(3,5\text{-}Me_2C_6H_3)$ (C_6D_6, 600 MHz).

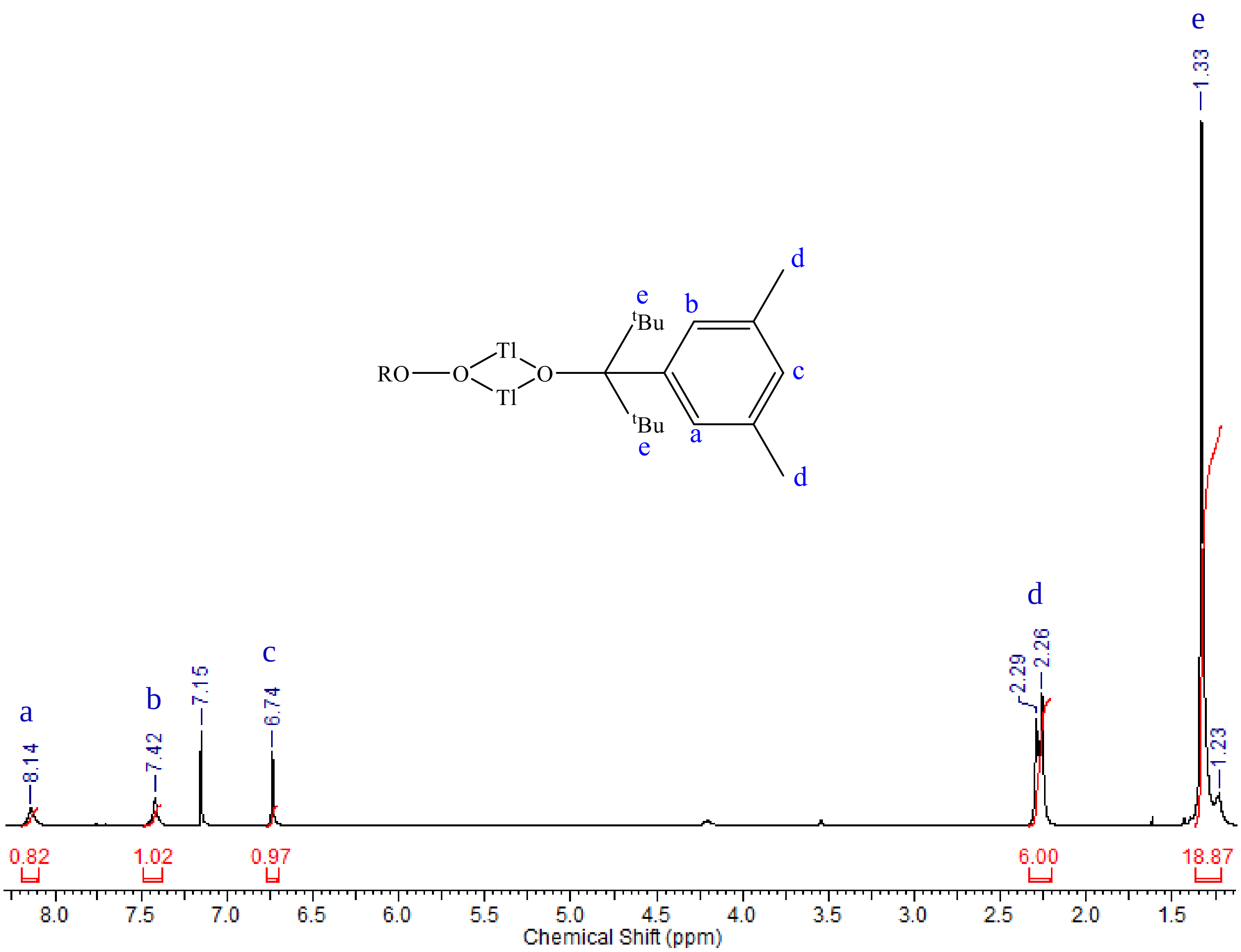

Figure S24. [1]H NMR of $TlOC^{t}Bu_2(3,5\text{-}Me_2C_6H_3)$ (C_6D_6, 600 MHz) (single isomer, obtained after prolonged storage at -35 °C).

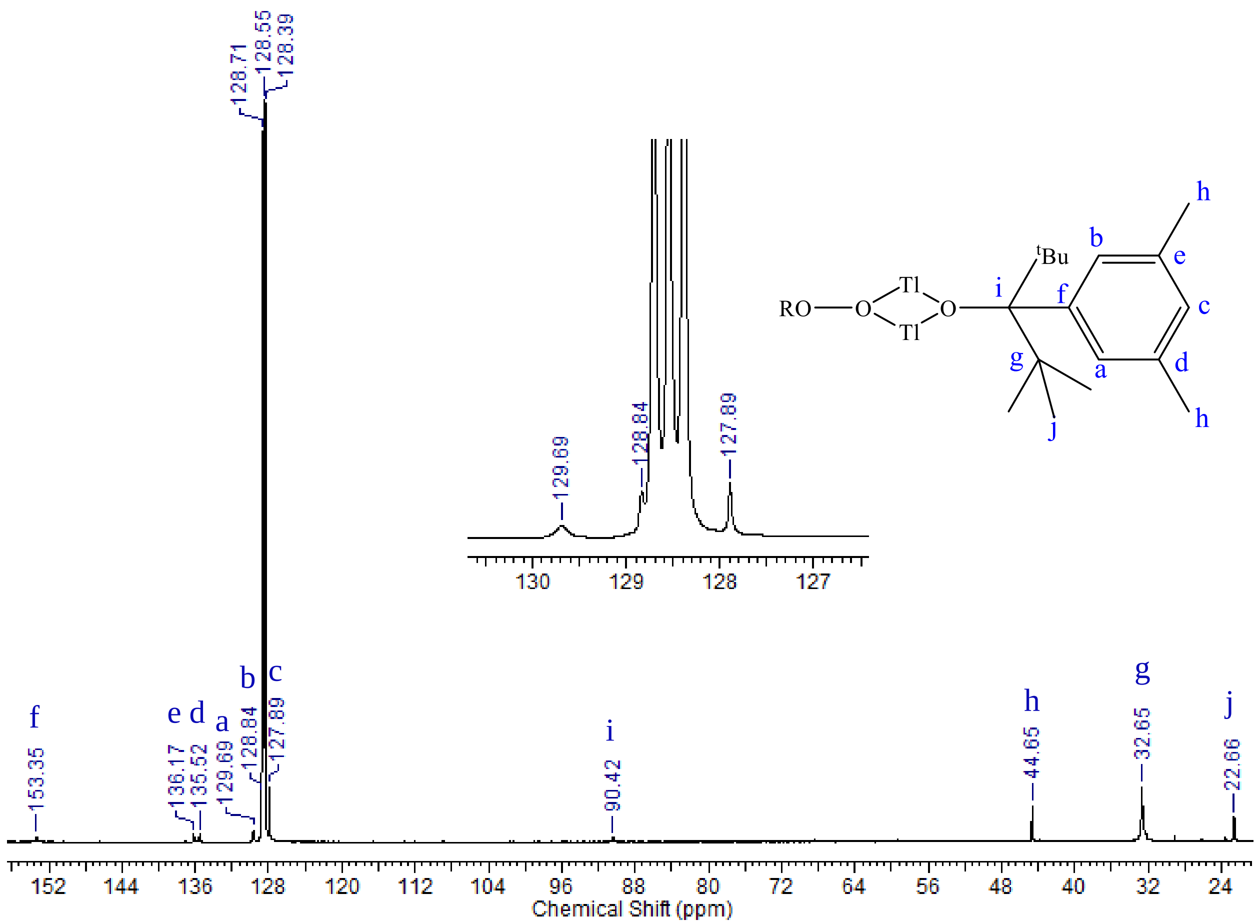

Figure S25. ^{13}C NMR of $TlOC^tBu_2(3,5\text{-}Me_2C_6H_3)$ (C_6D_6, 150 MHz).

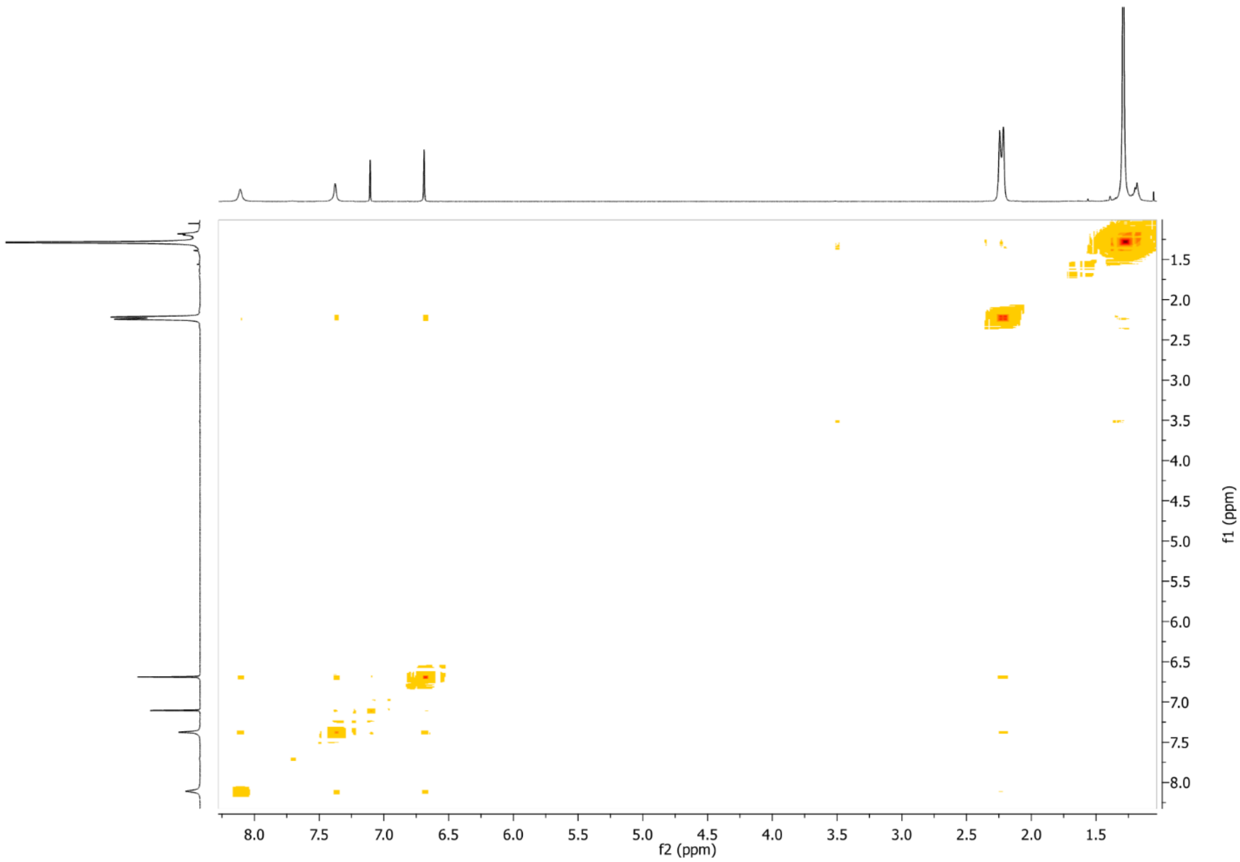

Figure S26. ^1H-^1H COSY NMR of $TlOC^tBu_2(3,5\text{-}Me_2C_6H_3)$ (C_6D_6, 600 MHz).

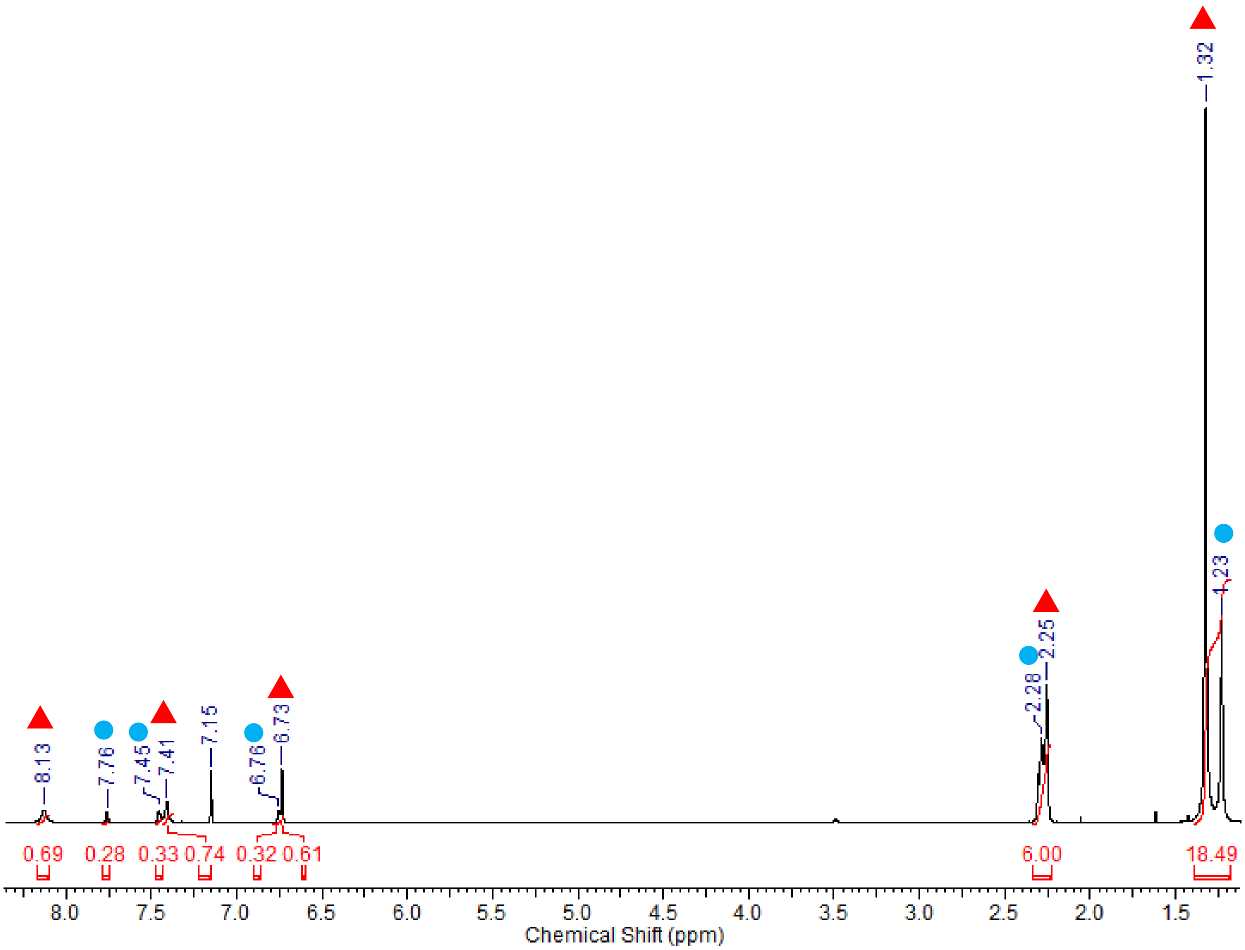

Figure S27. [1]H NMR of freshly prepared $Tl_2(OC^tBu_2(3,5\text{-}Me_2C_6H_3))_2$ (C_6D_6, 600 MHz, room temperature) demonstrating two isomers.

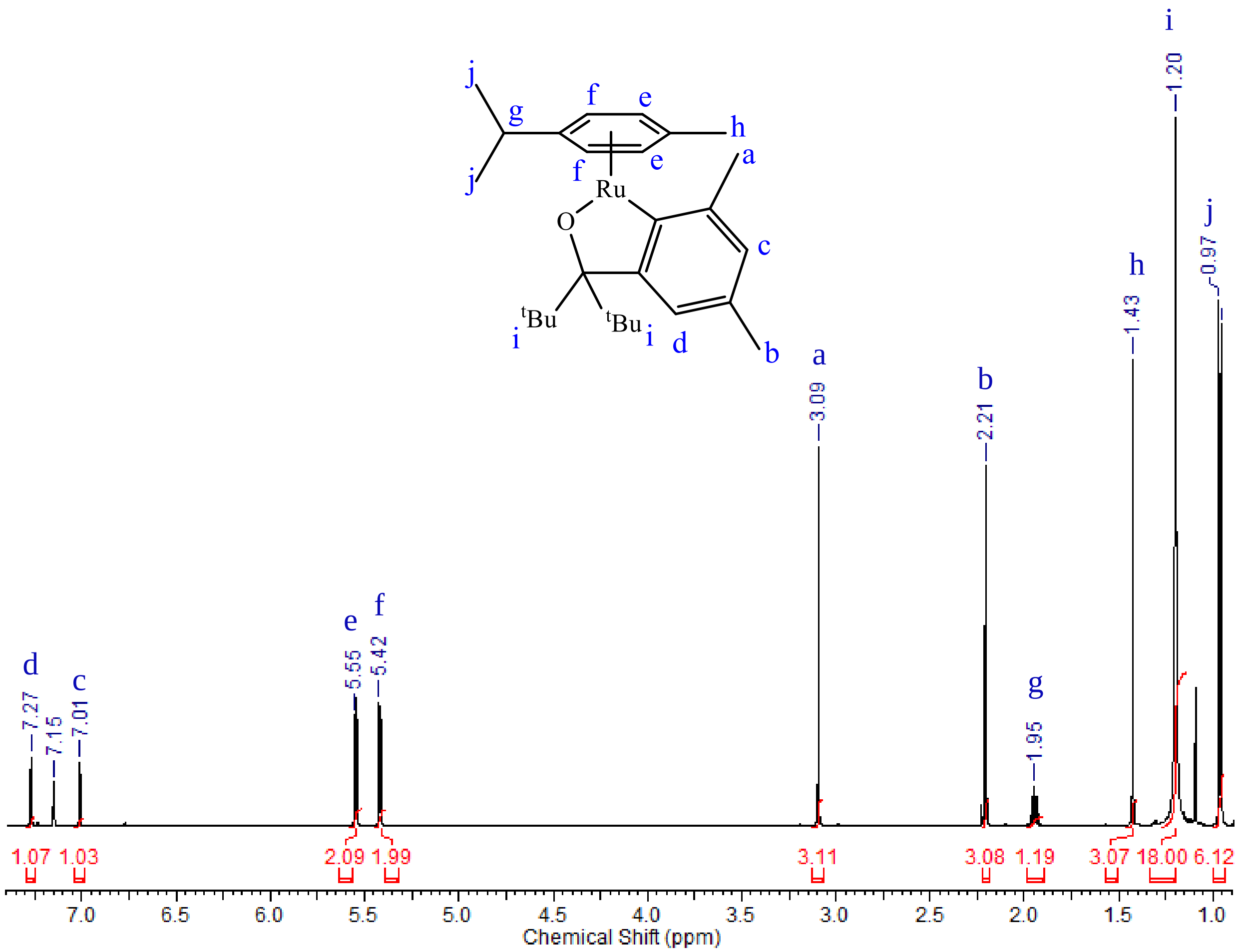

Figure S28. ^{1}H NMR of Ru(cymene)(κ^2-OC^{t}Bu$_2$(3,5-Me$_2$C$_6$H$_3$)) (C$_6$D$_6$, 600 MHz).

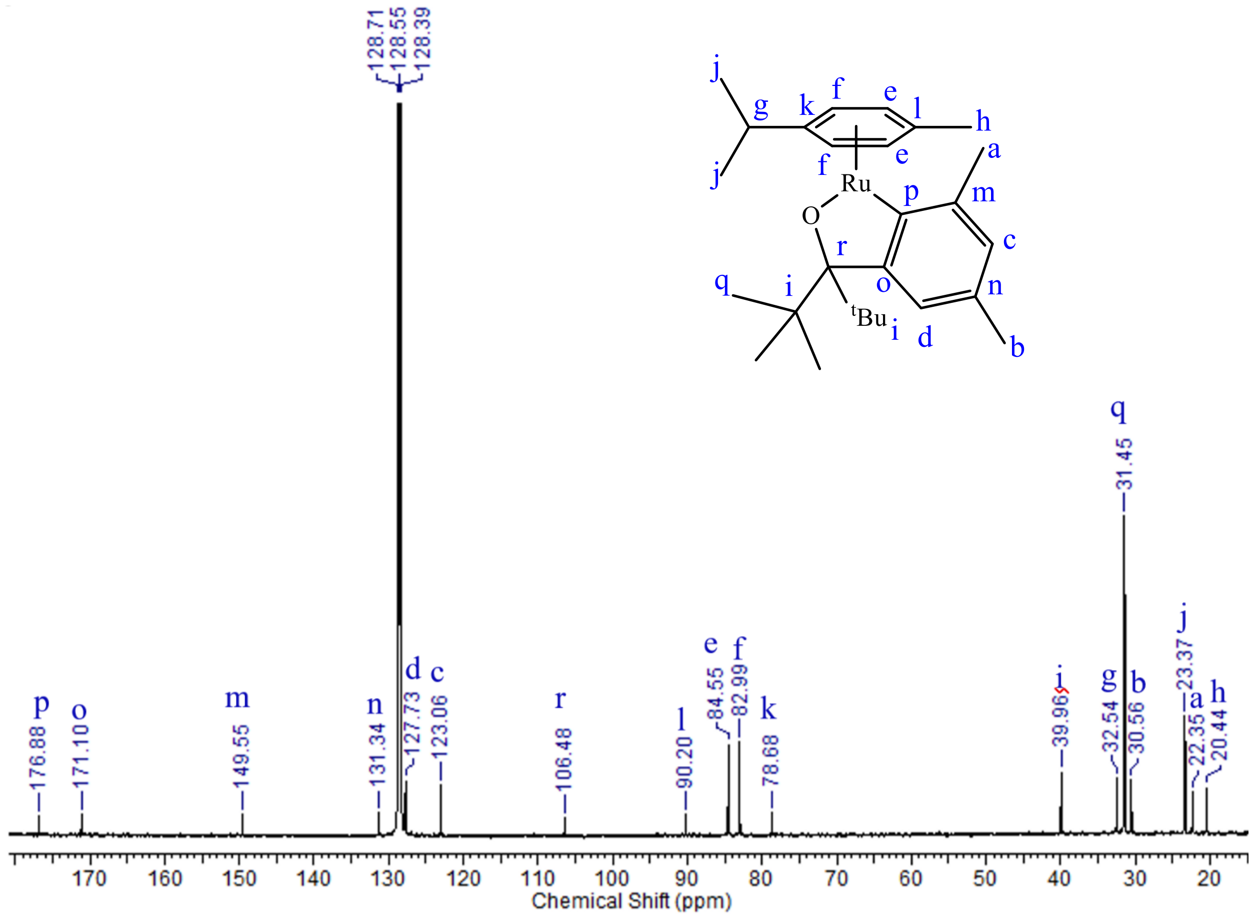

Figure S29. ^{13}C NMR of Ru(cymene)(κ^2-OC ^{t}Bu$_2$(3,5-Me$_2$C$_6$H$_3$)) (C$_6$D$_6$, 150 MHz).

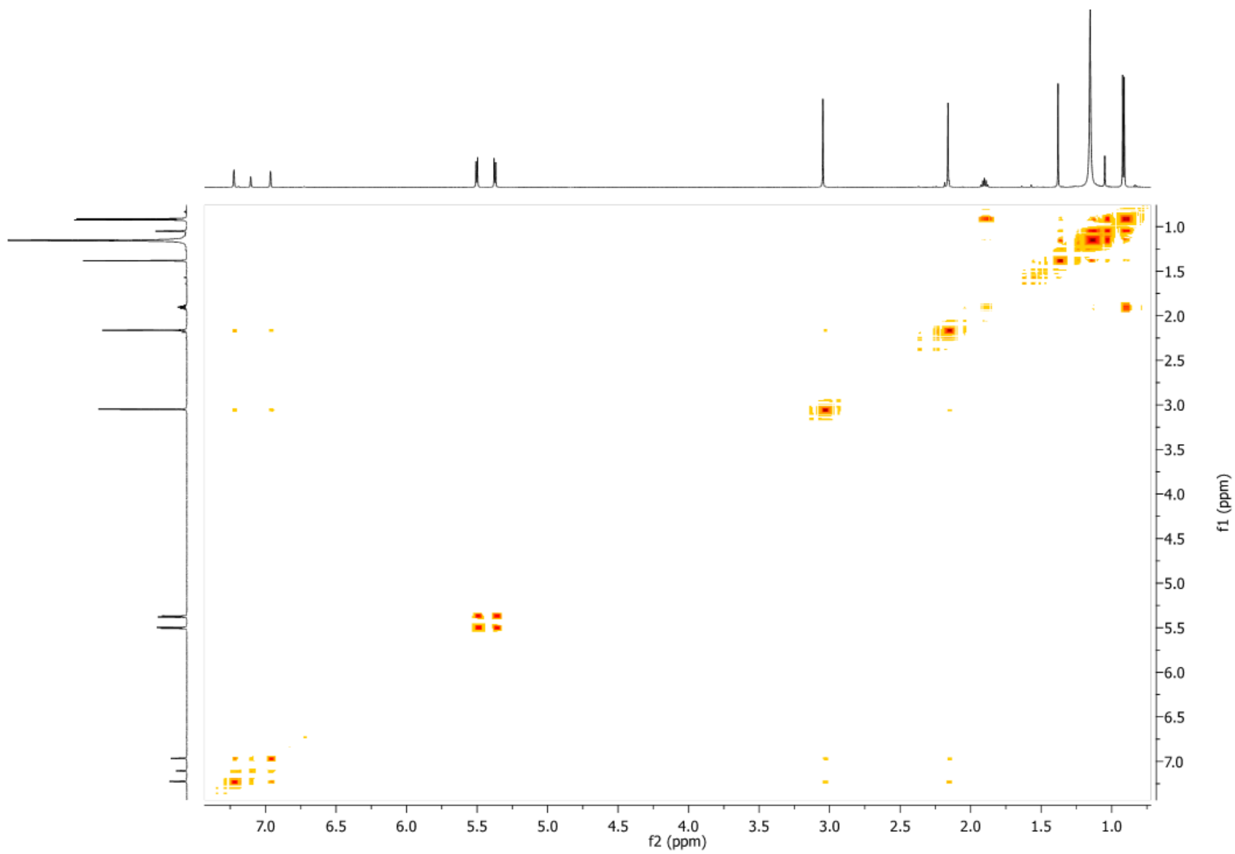

Figure S30. ^{1}H-^{1}H COSY NMR of Ru(cymene)(κ^2-OC ^{t}Bu$_2$(3,5-Me$_2$C$_6$H$_3$)) (C$_6$D$_6$, 600 MHz).

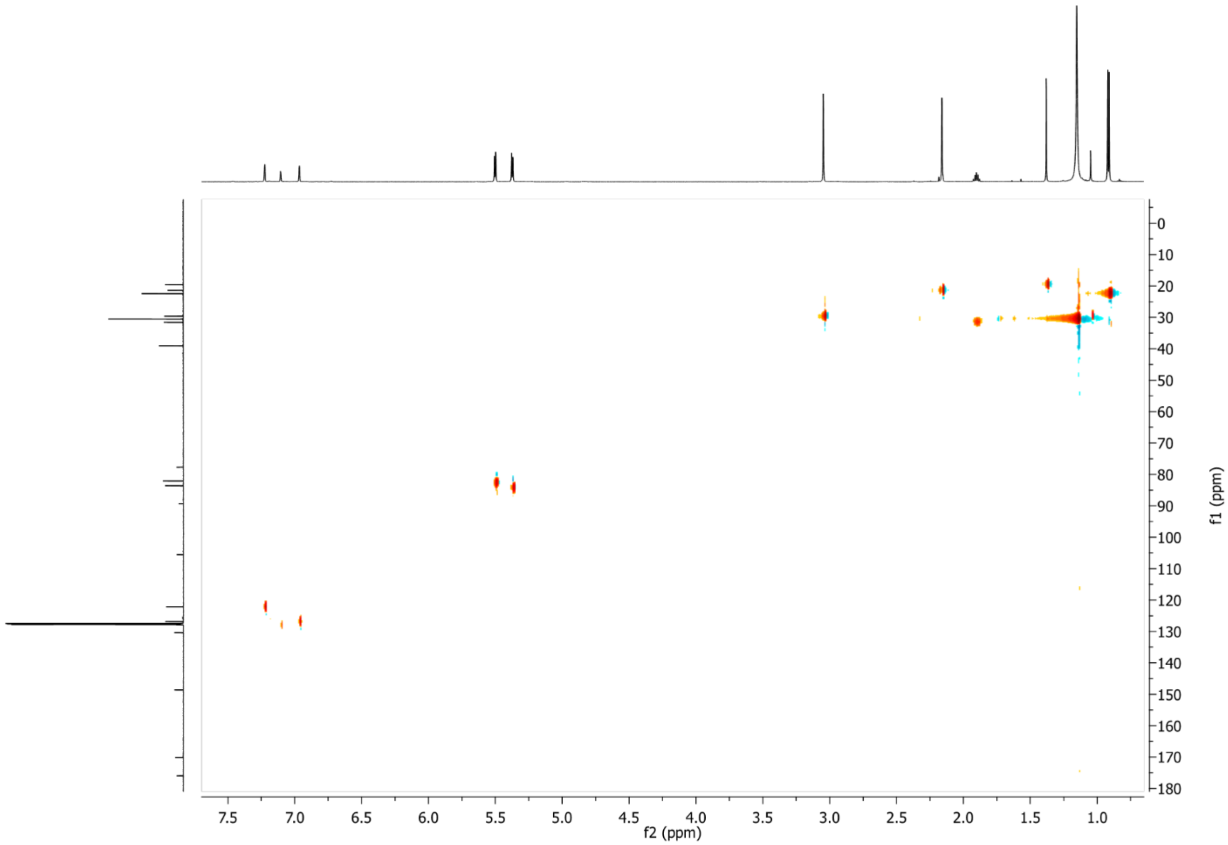

Figure S31. ^{1}H-^{13}C HSQCAD NMR of Ru(cymene)(κ^2-OC ^{t}Bu$_2$(3,5-Me$_2$C$_6$H$_3$)) (C$_6$D$_6$, 600 MHz).

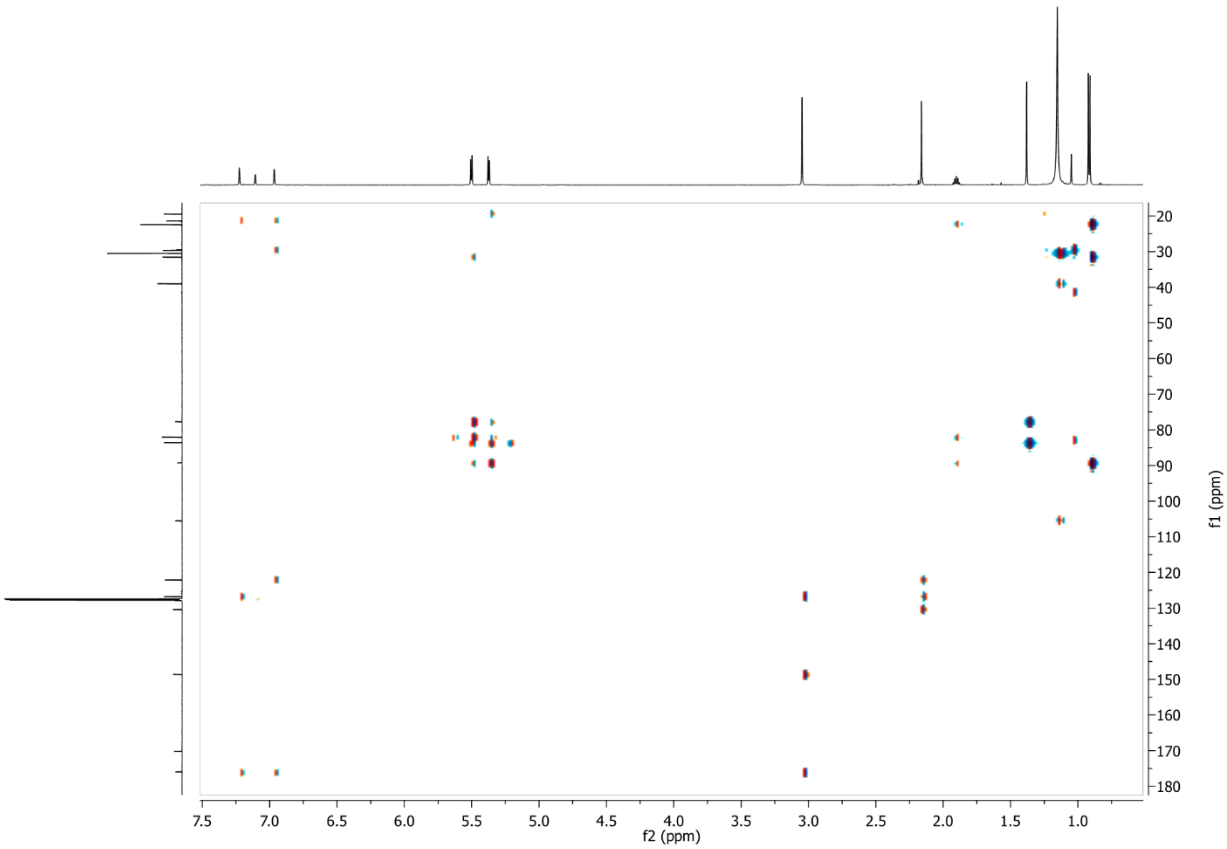

Figure S32. ^{1}H-^{13}C HMBCAD NMR of Ru(cymene)(κ^2-OC ^{t}Bu$_2$(3,5-Me$_2$C$_6$H$_3$)) (C_6D_6, 600 MHz).

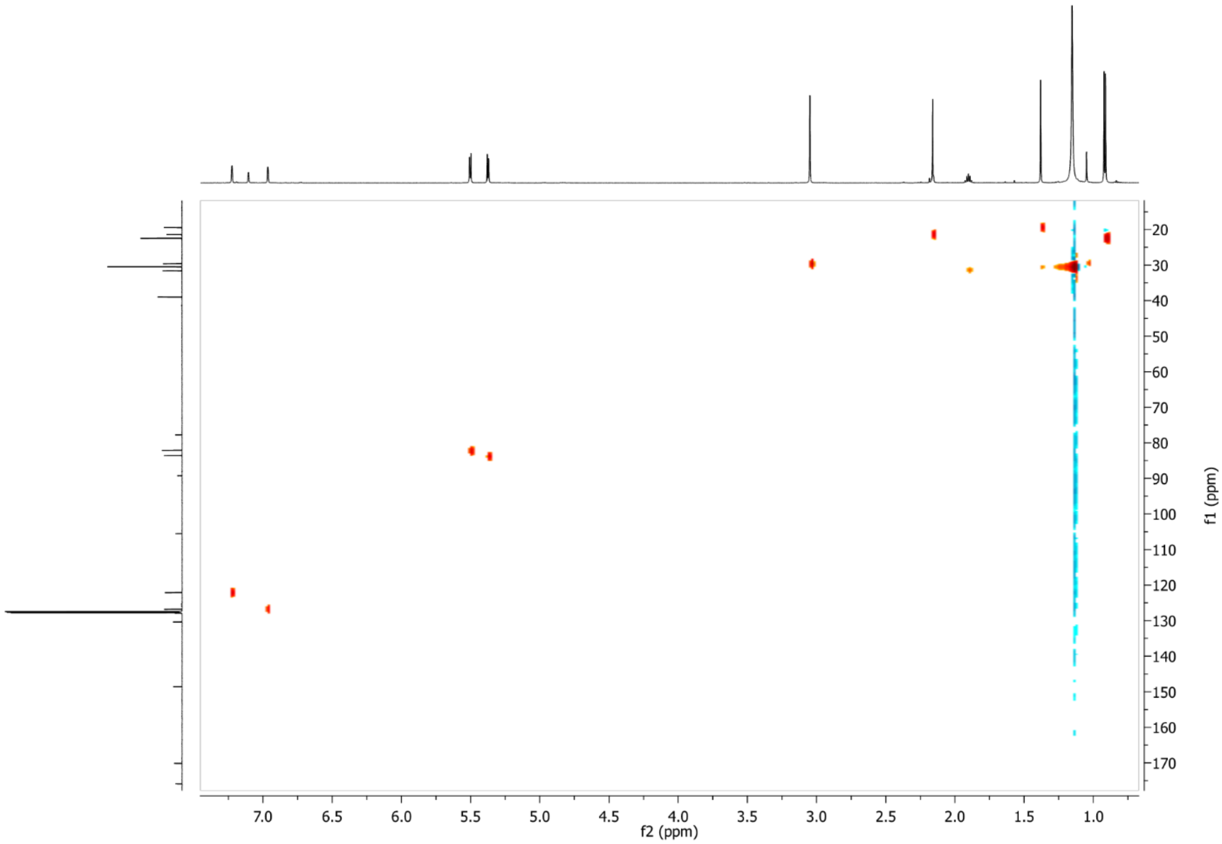

Figure S33. ^{1}H-^{13}C HMQC NMR of Ru(cymene)(κ^2-OC^{t}Bu$_2$(3,5-Me$_2$C$_6$H$_3$)) (C_6D_6, 600 MHz).

2. UV-Vis Spectra

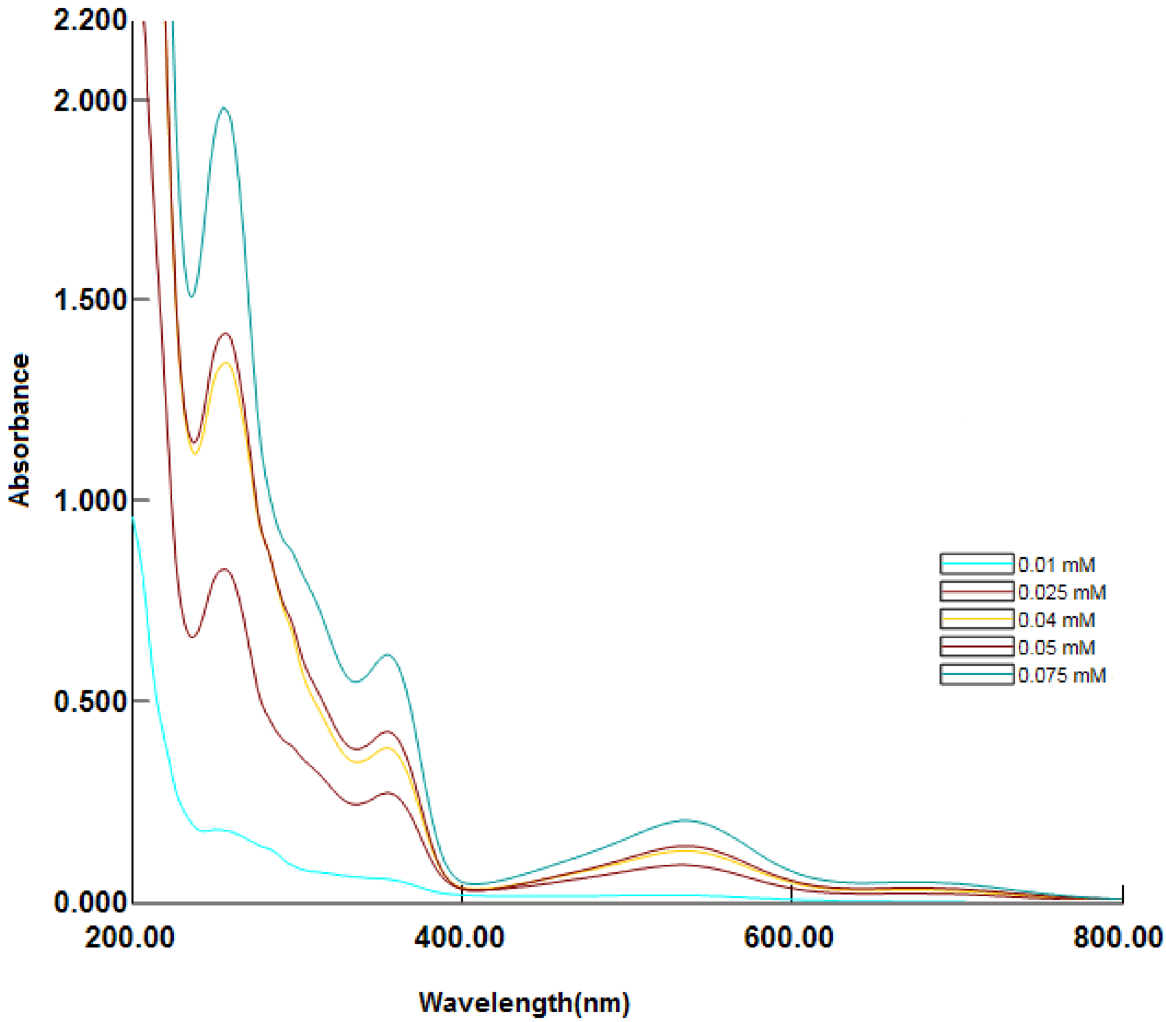

Figure S34. UV-Vis spectra for Ru(cymene)(κ^2-OC^{t}Bu$_2$C$_6$H$_2$) at five different concentrations. λ_{max}, nm (ε_M, L mol^{-1} cm^{-1}): 539 (2800), 355 (8600), 296 (sh, 13400), 256 (28300).

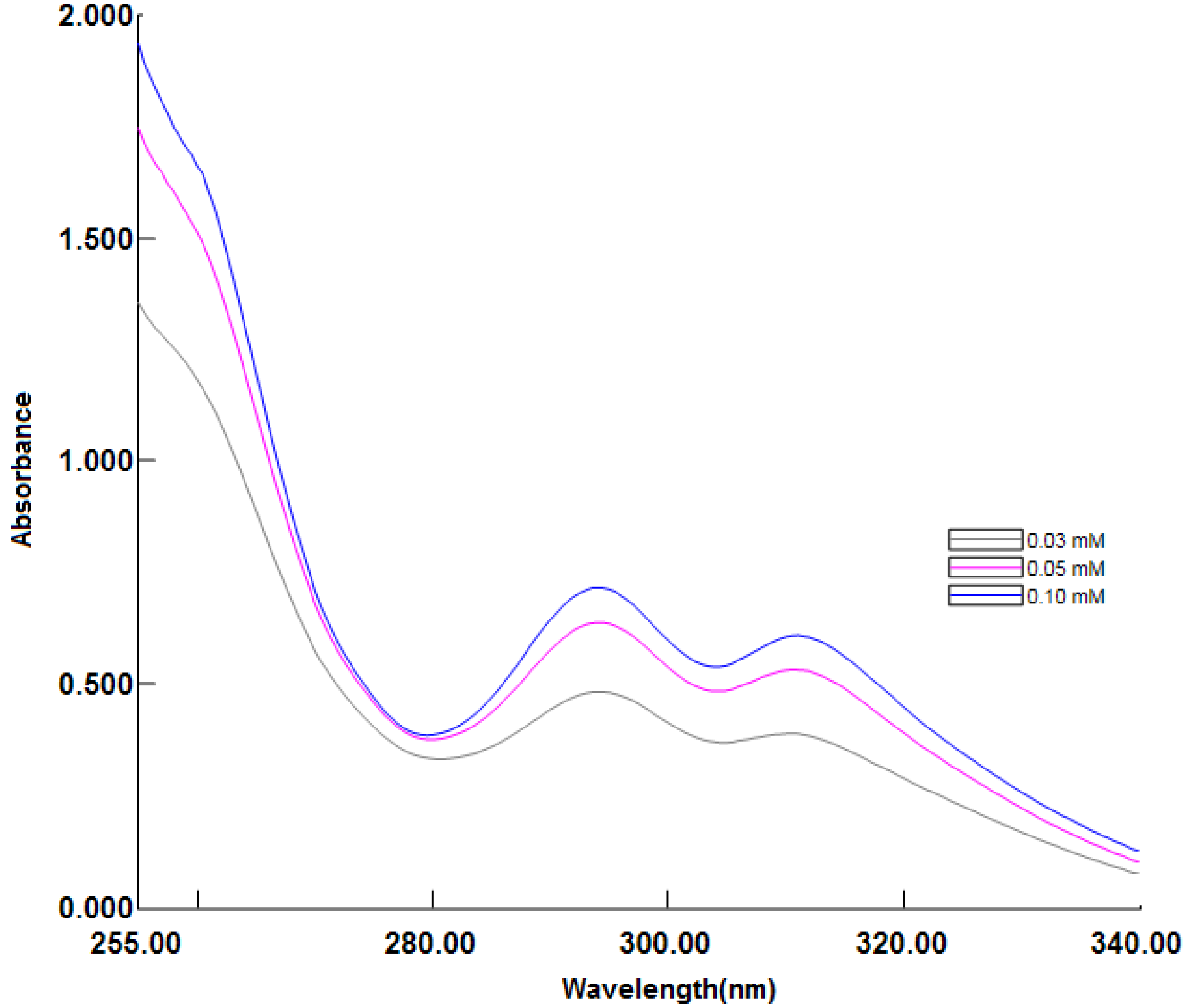

Figure S35. UV-Vis spectrum for $Tl_2(OC^tBu_2Ph)_2$ at three different concentrations. λ_{max}, nm (ε_M, L mol^{-1} cm^{-1}): 311 (3100), 294 (3300), 261(sh, 6500).

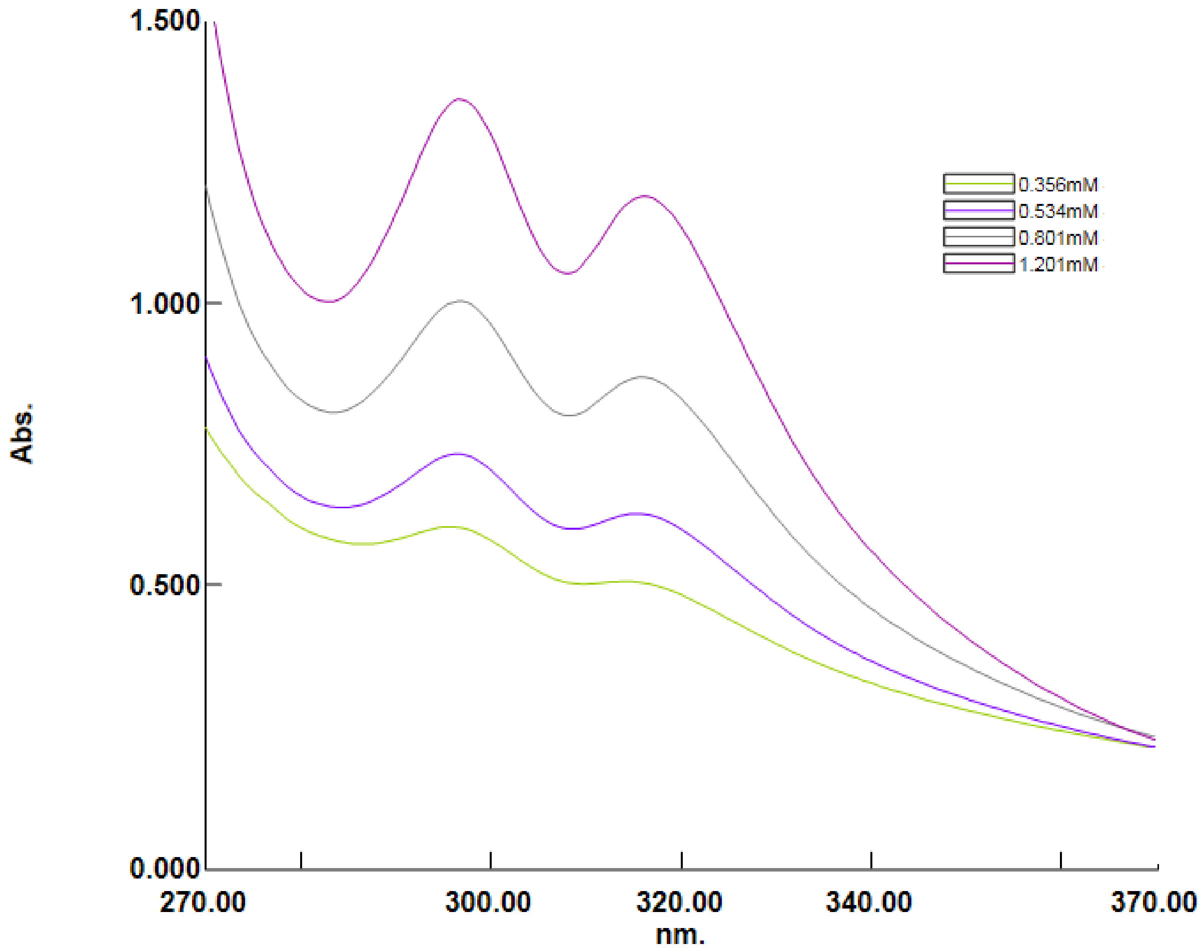

Figure S36. UV-Vis spectrum for $Tl_2(OC^tBu_2(3,5\text{-}Me_2C_6H_3))_2$ at four different concentrations. λ_{max}, nm (ε_M, L mol^{-1} cm^{-1}): 316 (900), 297 (1200).

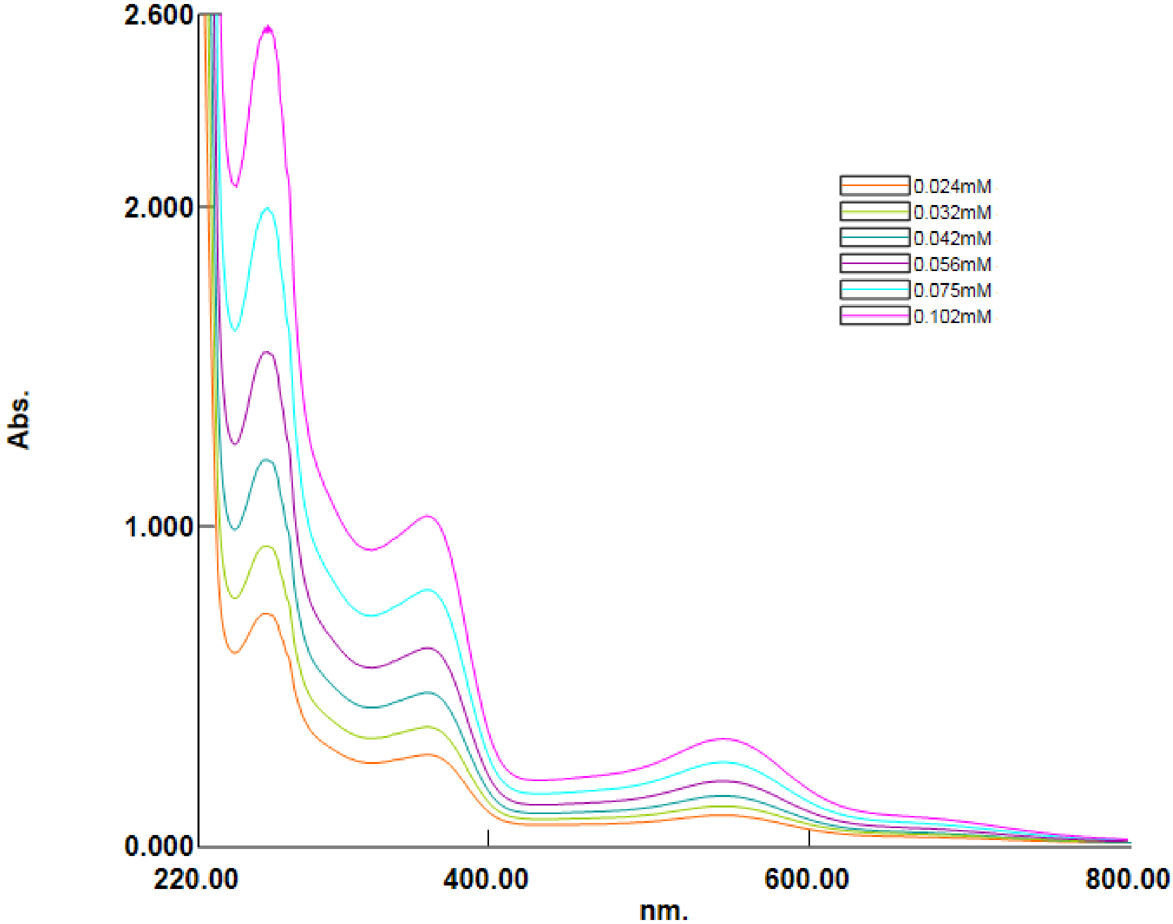

Figure S37. UV-Vis spectra for Ru(cymene)(κ^2-OC^{t}Bu$_2$(3,5-Me$_2$C$_6$H$_3$)) at six different concentrations. λ_{max}, nm (ε_M, L mol^{-1} cm^{-1}): 545 (5200), 361 (15400), 263 (30000).

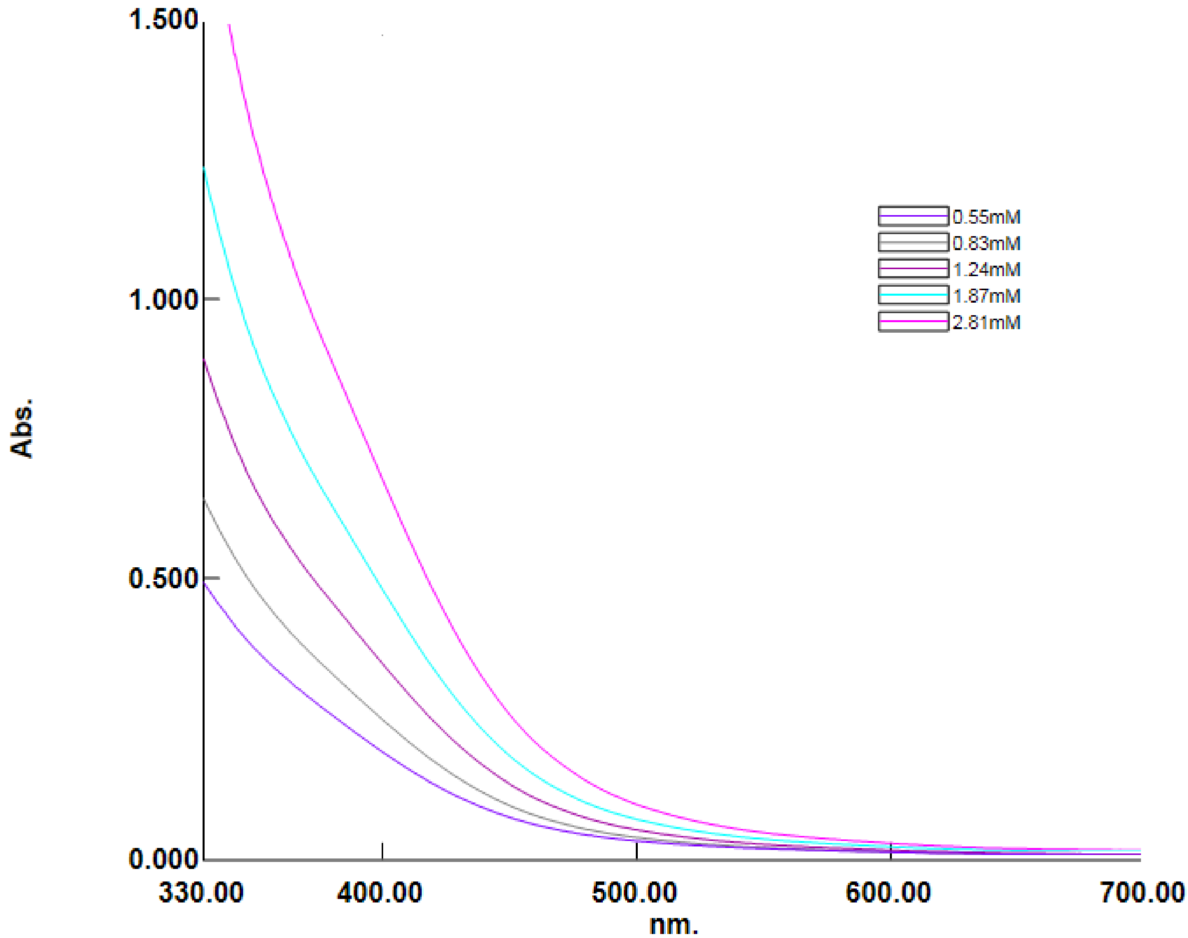

Figure S38. UV-Vis spectrum of $Fe(OC^{t}Bu_2(3,5\text{-}Me_2C_6H_3))_2(THF)_2$ at five different concentrations. λ_{max}, nm (ε_M, L mol^{-1} cm^{-1}): 407 (sh, 250).

3. IR Spectra

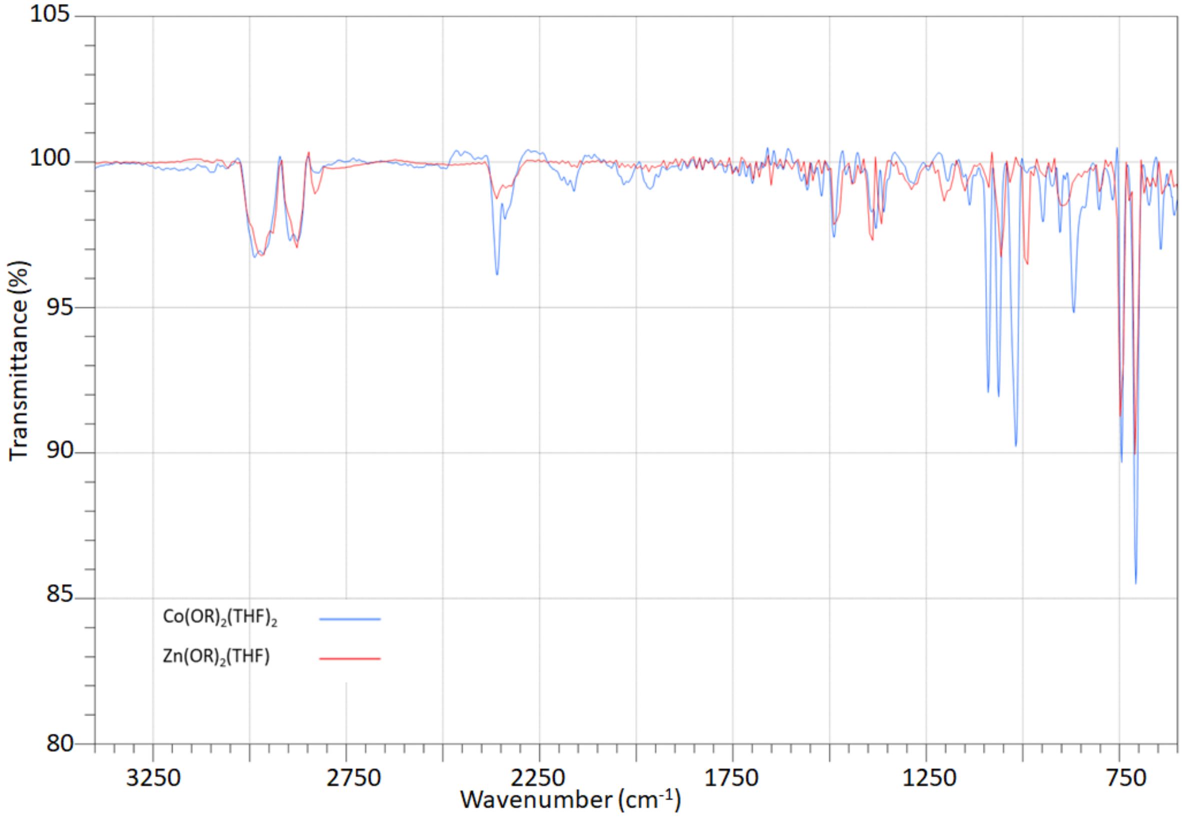

Figure S39. Overlaid IR spectra of Co(OC^{t}Bu$_2$Ph)$_2$(THF)$_2$ and Zn(OC^{t}Bu$_2$Ph)$_2$(THF) in the 3400-600 cm^{-1} range.

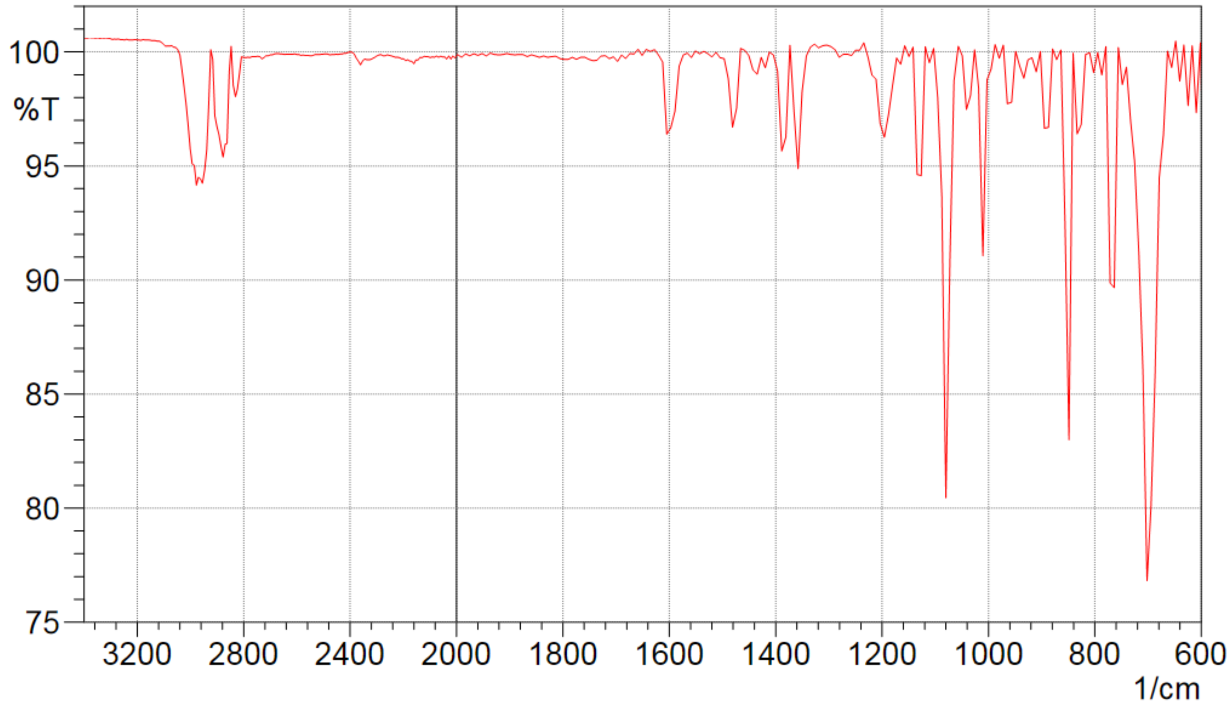

Figure S40. IR spectra of $LiOC^{t}Bu_2(3,5\text{-}Me_2C_6H_3)$ in the 3400-600 cm^{-1} range.

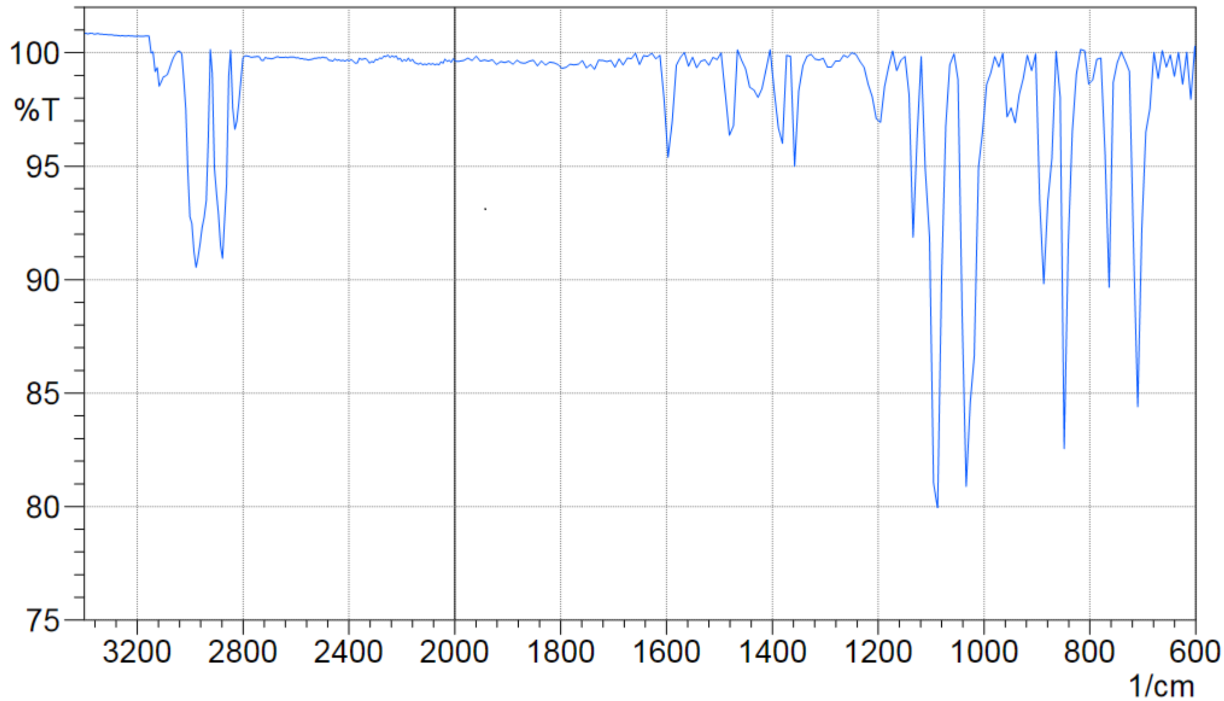

Figure S41. IR spectra of $Fe(OC^tBu_2(3,5\text{-}Me_2C_6H_3))_2(THF)_2$ in the 3400-600 cm^{-1} range.

4. ORTEP plots of 1a and 1b demonstrating agostic interactions

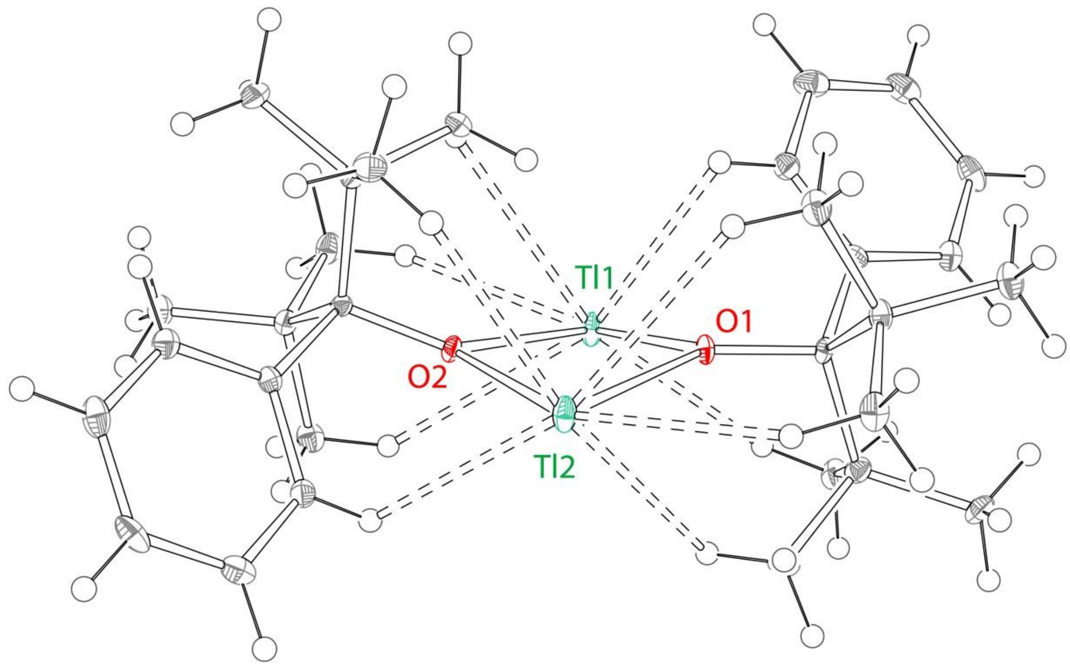

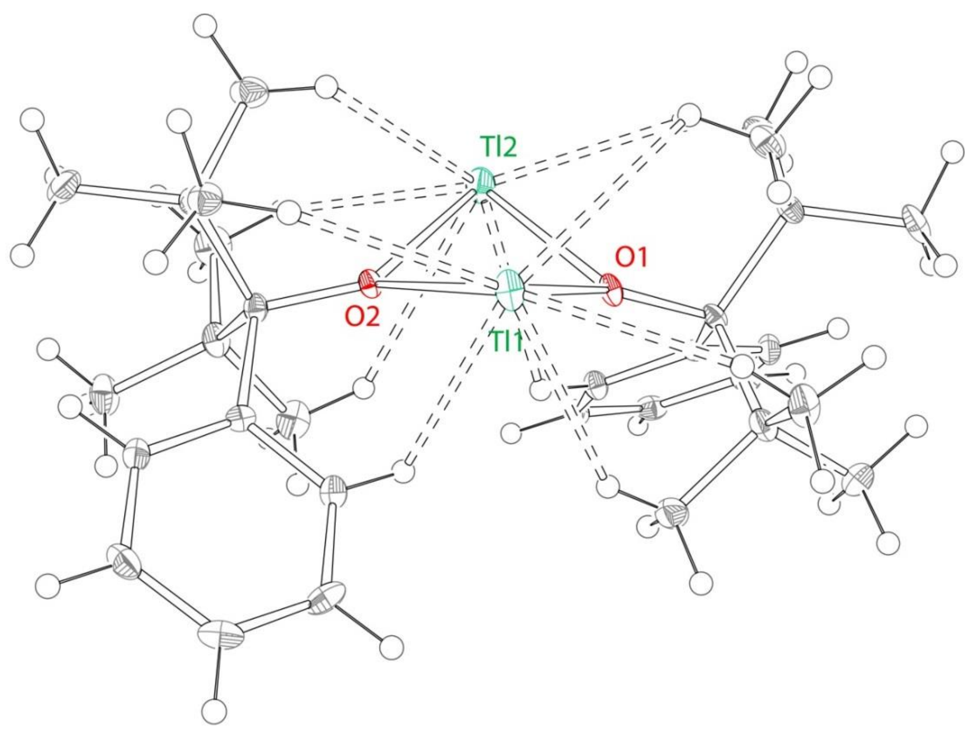

Figure S42. ORTEP diagram (50% probability ellipsoids) demonstrating agostic interactions for **1a** (top) and **1b** (bottom). Tl···H-C bond lengths are in 2.7-3.0 Å range.

5. X-ray structure of $LiOC^tBu_2(3,5\text{-}Me_2C_6H_3)$ (7)

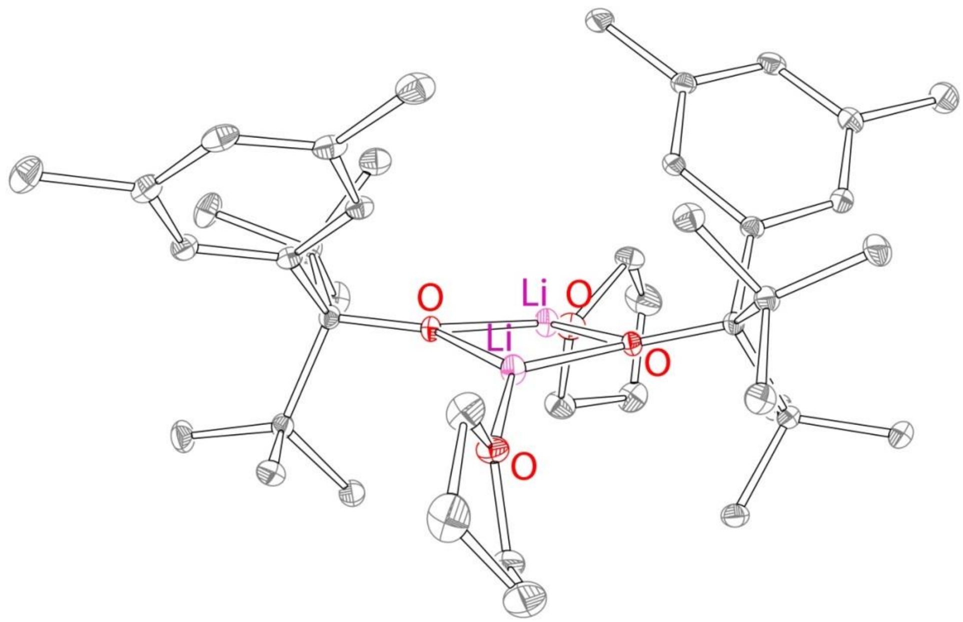

Figure S43. ORTEP diagram (50% probability ellipsoids) of the X-ray structure of **7**. H atoms were omitted for clarity.

6. Table S1. Crystal and structure refinement data.

	1a	**1b**	**5**	**6**
Formula	$C_{30}H_{46}O_2Tl_2$	$C_{30}H_{46}O_2Tl_2$	$C_{34}H_{54}O_3Zn$	$C_{25}H_{36}ORu$
Fw, g/mol	847.41	847.41	576.14	453.61
temperature	100(2) K	100(2) K	100(2) K	100(2) K
cryst syst	Triclinic	triclinic	monoclinic	triclinic
space group	*P-1*	*P-1*	$P2_1/n$	*P-1*
Colour	colorless	bright yellow	colorless	purple
Z	2	2	2	2
a, Å	7.9029(9)	8.0763(5)	10.0341(11)	9.3633(8)
b, Å	12.1061(14)	12.3094(7)	23.577(3)	11.1104(9)
c, Å	15.5684(18)	15.4883(9)	13.7200(17)	11.4477(9)
α, deg	88.456(4)	101.592(2)	90.00	91.329(4)
β, deg	80.664(4)	94.016(3)	106.953(4)	102.082(4)
γ, deg	74.856(4)	105.845(2)	90.00	112.349(4)
V, A^3	1418.5(3)	1438.24(15)	3104.8(6)	1070.07(15)
d_{calcd}, g/cm^3	1.984	1.957	1.233	1.408
μ, mm^{-1}	11.369	11.214	0.822	0.744
2θ, deg	55.98	50.00	60.06	56.74
R_1[a] (all data)	0.0224	0.0315	0.1088	0.0354
wR_2[b] (all data)	0.0392	0.0675	0.1009	0.0697
R_1[a] [(I>2σ)]	0.0176	0.0262	0.0477	0.0319
wR_2[b] [(I>2σ)]	0.0376	0.0651	0.0835	0.0682
GOF (F^2)	1.024	1.151	1.000	1.108

[a] $R1 = \Sigma||F_o - |F_c||/\Sigma|F_o|$. [b] $wR2 = (\Sigma(w(F_o^2 - F_c^2)^2)/\Sigma(w(F_o^2)^2))^{1/2}$. [c] $GOF = (\Sigma\, w(F_o^2 - F_c^2)^2/(n - p))^{1/2}$ where *n* is the number of data and *p* is the number of parameters refined.

Table S1. Crystal and structure refinement data (continued).

	7	**8**	**9**	**10**
Formula	$C_{42}H_{70}O_4$ Li_2	$C_{34}H_{54}O_2Tl_2$	$C_{42}H_{70}O_4Fe$	$C_{27}H_{40}ORu$
Fw, g/mol	652.86	903.51	694.83	481.66
temperature	100(2) K	100(2) K	100(2) K	100(2) K
cryst syst	monoclinic	monoclinic	monoclinic	triclinic
space group	*P2₁/c*	*P2₁*	*P2₁/n*	*P-1*
Colour	colorless	colorless	colorless	violet
Z	4	2	4	2
a, Å	11.9523(13)	8.0476(3)	10.4095(5)	8.1664(4)
b, Å	21.215(3)	15.1435(6)	14.9890(7)	10.4284(5)
c, Å	15.9314(18)	13.6841(5)	25.9262(11)	14.7777(7)
α, deg	90.00	90.00	90.00	106.093(2)
β, deg	93.335(5)	98.9240(10)	96.890(2)	98.321(2)
γ, deg	90.00	90.00	90.00	93.777(2)
V, A^3	4032.9(9)	1647.48(11)	4016.0(3)	1189.00(10)
d_{calcd}, g/cm^3	1.075	1.821	1.149	1.452
μ, mm^{-1}	0.066	9.796	0.413	0.674
2θ, deg	55.84	55.14	49.70	61.18
R_1[a] (all data)	0.0589	0.0312	0.1070	0.0367
wR_2[b] (all data)	0.1126	0.0519	0.1063	0.0762
R_1[a] [(I>2σ)]	0.0422	0.0264	0.0516	0.0303
wR_2[b] [(I>2σ)]	0.1027	0.0503	0.0910	0.0734
GOF (F^2)	1.034	1.033	1.005	1.090

[a] $R1 = \Sigma||F_o - |F_c||/\Sigma|F_o|$. [b] $wR2 = (\Sigma(w(F_o^2 - F_c^2)^2)/\Sigma(w(F_o^2)^2))^{1/2}$. [c] GOF = $(\Sigma\, w(F_o^2 - F_c^2)^2/(n - p))^{1/2}$ where n is the number of data and p is the number of parameters refined.